Cost-optimized design of a dual-mode diesel parallel hybrid electric vehicle for several driving missions and market scenarios

Roberto Finesso, Ezio Spessa[1] and Mattia Venditti

IC Engines Advanced Laboratory, Dipartimento Energia, Politecnico di Torino

c.so Duca degli Abruzzi 24, 10129 - Torino, Italy

roberto.finesso@polito.it, ezio.spessa@polito.it, mattia.venditti@polito.it

Abstract

The present study has focused on the refinement of a previously developed tool for the optimization of the layout of hybrid electric vehicles and on its application to a newly proposed non-plug in parallel hybrid vehicle, which has been equipped with a planetary gear set and a single-speed gearbox positioned between a compression ignition engine and a permanent magnet electric machine. This vehicle is capable of torque-coupling and speed-coupling between the engine and the electric machine, and for this reason has been referred to as a "dual-mode vehicle".

The tool performs a bi-level (nested) coupling of design and control strategy optimization, and is able to identify the optimal design of each hybrid vehicle by minimizing the powertrain costs over a 10-year time span. The vehicle design determines the size of battery, engine and electric machine, as well as the values of the speed ratio of each power coupling device. Different powertrain cost definitions, which account for the production costs of the components and the operating costs related to fuel consumption and battery depletion over the lifetime of the vehicle, have been proposed. The latter cost contribution depends directly on the control strategy adopted to manage the power flow between the electric machine and the engine, as well as on the selection of the

[1]Corresponding Author: Tel. +39-011.090.4482; Fax: +39-011.090.4599; e-mail: ezio.spessa@polito.it

transmission gear. The optimal control strategy has been identified using a specifically developed fast running dynamic programming-based optimizer, which minimizes an objective function over a given training driving mission.

The performance of the dual-mode vehicle with the optimal layout has been investigated in detail over several driving missions and compared with that of more traditional hybrid vehicles equipped with either a speed coupling device or with a torque coupling device, as well as with a conventional reference vehicle.

Moreover, several sensitivity analyses have been carried out in order to investigate the impact of the cost definition, of the objective function and of the training driving mission on the powertrain design and on its performance (fuel economy, pollutant emissions, battery management).

Finally, different market scenarios have been explored, in terms of fuel price, battery life and battery cost, and their effects on the identification of the optimal design, as well as on the performance of the resulting vehicles, have been analyzed.

Key Words: parallel hybrid vehicle; planetary gear; layout; cost-optimized design; market scenario

Nomenclature

Acronyms

AER: All Electric Range

AMDC: Artemis Motorway Driving Cycle

AUDC: Artemis Urban Driving Cycle

BLC: Battery Life Consumption

BU: Battery Usage

CO_2: Carbon dioxide

DMV: Dual Mode Vehicle

DP: Dynamic Programming

D1: 1.7 L Euro 5 GM diesel engine

D2: 1.3 L Euro 5 GM diesel engine

E: Engine

EGR: Exhaust Gas Recirculation

EM: Electric Machine

ES: Engine State

EV: Electric vehicle

FC: Fuel consumption

FD: Final Drive

GB: Gear Box

GN: Gear Number

HEV: Hybrid Electric Vehicle

J: Objective function

NOx: Nitrogen oxides

PF: Power Flow

PG: Planetary Gear set

PI: Performance Index

SC: Speed Coupling

SCV: Speed Coupling Vehicle

SOC: State Of Charge

TC: Torque Coupling

TCV: Torque Coupling Vehicle

TM1: Internally-developed Training Mission (1)

TM2: Internally-developed Training Mission (2)

TM3: Internally-developed Training Mission (3)

TR: Transmission

Variables

C: Cost [$]

C_{bat}: Battery capacity [Ah]

E: Energy [J]

I_{wh}: Wheel moment of inertia [kg m^2]

I_{bat}: Battery current [A]

$\dot{m}_{fc}$: Fuel mass flow rate [kg/s]

$\dot{m}_{co2}$: CO2 mass flow rate [kg/s]

P_{fd}: Final drive power [W]

P_v: Vehicle power [W]

R_{wh}: Dynamic radius of the wheel [m]

S_{es}: Set of discrete values of the state of the engine

S_{gn}: Set of discrete values of GN

S_{pf}: Set of discrete values of PF

S_{soc}: Set of discrete values of SOC

t: Time [s]

T: Torque [Nm]

u: control strategy

V_v: Velocity [m/s]

Greek symbols

α: Sub-control variable of PF

λ: Battery life consumption [Ah]

λ_r: Battery life residual [-]

Λ: Battery life [Ah]

ρ: Fuel density [kg/m^3]

σ: Severity factor related to battery aging [-]

τ_{sc}: Speed ratio of the speed coupling device [-]

τ_{tc}: Speed ratio of the torque coupling device [-]

ω: Angular speed [rad/s]

1. Introduction

1.1 Background

In recent years, the automotive industry has dedicated a great deal of effort to developing innovative technologies for the realization of green vehicles characterized by low CO2 and pollutant emissions [1]. Battery equipped electric vehicles (EV) have only a battery as the energy source, and traction power is provided by one or several electric machines. These vehicles are highly energy efficient and feature zero tailpipe emissions, while the well-to-wheel emissions depend on the electric energy production process. If the electric energy is derived from a renewable source, well-to-wheel emissions can be reduced to a great extent [2, 3]. However, these vehicles have not been successful so far on the market, because of the higher costs, the added weight of the batteries, the reduced load capacity, the limited driving range and the lack of recharging infrastructures [4]. Fuel-cell electric vehicles are still in their early stages of development, as the fuel-cell technology is not yet mature, but they have shown an interesting long-term potential [2, 5]. Hybrid electric vehicles (HEVs) offer improved fuel economy and lower emissions than conventional vehicles and they can take advantage of existing fuel infrastructures. HEVs are provided with two energy sources, i.e., a battery and a fuel tank, and they are equipped with a conventional thermal engine and one or several electric machines. A significant advantage of HEVs, compared to battery EVs, is that they offer the possibility of increasing the driving range, due to the presence of the thermal engine. However, the driving range in pure electric mode is much lower, as a consequence of the installation of smaller battery packs. HEVs lead to a reduction in fuel consumption (FC) and CO2 emissions, compared to conventional vehicles, mainly due to the reduction in engine size, to the possibility of recovering

the kinetic energy through regenerative braking, to the implementation of the Stop-Start mode and to the possibility of optimizing the power flow from the engine and electric machines [6]. Several studies have demonstrated the capacity of the hybrid technology to reduce CO2 emissions in developing countries [7, 8], which are expected to contribute significantly to the greenhouse gas emissions from the transport sector in the near future. Moreover, a recent study has shown that the life cycles of CO2 emissions of modern HEVs are shorter than those of conventional vehicles [9]. HEVs are therefore considered to represent one of the most promising technologies. A classification of HEVs can first be made considering whether the batteries can be charged from an electric grid (plug-in HEVs) or not (non plug-in HEVs). Plug-in hybrid electric vehicles use both electrochemical energy storage and a conventional fuel to overcome the drawbacks of EVs and HEVs. Plug-in HEVs have the potential of further reducing fuel consumption, as well as pollutant and CO2 emissions, compared to non-plug-in HEVs [10-12]. However, they are usually equipped with larger battery packs than non plug-in HEVs, in order to allow a higher all-electric range (AER) to be obtained. Moreover, the incremental battery cost of plug-in HEVs might not be counterbalanced by the savings in fuel cost, as was shown in [13].

HEVs can also be classified according to their architecture. Many different hybrid architectures, whether of a series, parallel or complex series/parallel type [9], have been developed by car manufacturers. The parallel architecture is currently one of the most frequently adopted ones in hybrid vehicles. In this kind of architecture, both the engine and electric machine supply mechanical power directly to the driven wheels. The role of the electric machine is therefore to assist the engine to operate efficiently and to recover energy through regenerative braking. The main advantages of a parallel configuration over a series configuration are that a generator is not required, the electric machine used for traction is smaller, and multi-conversion of the power from the engine to the driven wheels is not necessary. The parallel configuration may have several configurations, which depend on the connection between the transmission, the electric machines and the engine.

The key-aspects that should be considered to fully exploit the capacity of HEVs to reduce CO2 and pollutant emissions are the design definition and energy management, i.e., the identification of the optimal control strategy during vehicle operation. Only a few studies have been found in the literature, which addressed to the co-design process of hybrid vehicles.

Four different types of coupling between the plant and controller optimization problem were examined in [14], that is, sequential, iterative, bi-level (nested) and simultaneous types. The nested and simultaneous coupling strategies were found to offer the best performance as they guarantee system-level optimality.

A methodology for the optimization of plug-in HEV component sizing, using a parallel chaos optimization algorithm, is described in [4].

Optimization of powertrain component sizing and of the control strategy was studied in [15] for a fuel cell hybrid electric bus. A higher fuel economy and minimum powertrain costs were achieved using a multi-objective genetic algorithm with preset design variables and vehicle performance constrains.

A combined power management/design optimization problem for the optimization of fuel cell/battery hybrid vehicles was formulated in [16]. Subsystem-scaling models were utilized to predict the component size and were integrated into a stochastic-dynamic-programming controller design process.

The study in [17], like that in [15], demonstrated the system-control co-design of a fuel cell/battery/super-capacitor vehicle using a multi-objective genetic algorithm. The optimization process was based on the minimization of fuel consumption, while preserving the battery state of charge under different driving cycles.

A sequential-type co-design for a fuel cell/battery/super-capacitor hybrid electric vehicle was developed in [18]. In this case, the component sizing was first designed to meet the performance constraints of a vehicle. A real-time optimization of the power flow of the three powertrain components was then carried out.

A rule-based control is a technique that is used extensively in hybrid systems to obtain an optimal energy management [19]. This method is characterized by simple implementation, high computational efficiency and fast experimental verification. However, it is not suitable for complicated or highly non-linear systems, due to its inherent drawback, i.e., an engineering intuition-based design. In order to deal with such problems, as well as to enhance robustness against system uncertainties, the fuzzy logic control method is often applied for various types of hybrid systems [20]. However, the main problem of these methods is that a system with numerous control variables could lead to a large number of logic rules.

An alternative method for the control strategy optimization of systems equipped with dual energy (or power) sources is based on the minimization of an equivalent energy [21]. This is also known as a “static optimization

172 method". The simulated results can be organized in the form of multi-dimensional tables, which can be coded
173 and downloaded directly to a control unit.
174 Dynamic Programming (DP) is a widely-used global optimization method that applies an exhaustive search for
175 the overall optimal control strategy under a predetermined driving cycle. This methodology was first introduced
176 by Bellman [22]. Its potentiality has been investigated in detail in several works [23, 24]. It has been found to be
177 a better candidate for the co-design of an optimal vehicle layout and control strategy than rule-based, fuzzy-
178 logic-based or static optimization methods. However, the DP-based tools that can be found in literature are very
179 time consuming. This drawback could represent a major concern for the adoption of such a technique.

180 1.2 Contribution of the present study

181 The main innovative contributions of this study, with reference to the background illustrated in the previous
182 section, are:
183 1. The refinement of a previously developed tool [25, 26] for the optimization of the layout of hybrid vehicles.
184 The tool is based on a bi-level (nested) approach, which has been found to offer the best performance when
185 the aim is to solve plant and controller optimization problems at the same time. Moreover, a DP-based
186 optimizer has been implemented to identify the optimal control strategy, as it leads to a global optimal
187 solution, which cannot be guaranteed by static optimizers or rule-based optimizers. However, the DP
188 optimizers currently available in the literature are very time consuming, and are therefore not suitable for
189 layout optimization applications, which require the investigation of a large number of possible layouts.
190 Therefore, specific mathematical techniques have been developed in order to set up a fast running DP-based
191 optimizer. The optimal control strategy has been identified by minimizing an objective function, which
192 accounts for fuel consumption, NOx emissions and battery life depletion, over a given mission profile.
193 The optimal vehicle design tool is based on the minimization of the powertrain cost over the lifetime of the
194 vehicle. Several cost definitions, which account for the component production costs and for the operating
195 costs related to fuel consumption and battery depletion, have been introduced. Most of the methodologies
196 proposed in the literature for vehicle design optimization are based on only fuel consumption minimization.

However, this approach may lead to aggressive battery employment, with a consequent impact on the operating costs.

The main novelties with respect to the tool presented in [26] are related to the introduction of new powertrain cost definitions (OEM cost, user cost, fuel cost, production cost, operating cost) and to the capability of performing different cost-oriented vehicle design optimizations.

2. The application of the refined tool to a newly proposed non-plug-in parallel hybrid electric vehicle, which has been equipped with a planetary gear set and a single-speed gearbox positioned between a compression ignition engine and a permanent magnet electric machine. This vehicle is capable of realizing torque-coupling and speed-coupling functions between the engine and the electric machine, and has therefore been referred to as a "dual-mode vehicle" (DMV). To the best of the authors' knowledge, this type of architecture has not yet been investigated in the literature, and seems highly promising in terms of fuel consumption and emission reduction. The DMV architecture in fact enables the engine operating point to be shifted either in terms of speed (via the planetary gear) or in terms of torque (via the single speed gearbox).
3. The comparison of the DMV performance with that of more traditional hybrid vehicles and with that of a reference conventional vehicle, over different driving missions, including two Artemis Driving Cycles (AUDC, AMDC) and three internally-developed training missions (TM1, TM2 and TM3). TM1 was developed to simulate the vehicle in a mountain-like scenario, TM2 to simulate highway-like conditions over different road slopes, and TM3 was developed in order to include a wide variation of driving conditions taken from several homologation cycles. Moreover, a study has been carried out to identify the architectures that show the best performance, in terms of NOx emission, CO2 emission and powertrain cost reductions, in different driving conditions.
4. A detailed sensitivity analysis, which has been conducted in order to investigate the impact of the cost definition, of the objective function and of the training driving mission on the powertrain design and on its performance (fuel economy, pollutant emissions, battery management, costs). Moreover, several indicators have been defined in order to estimate the incremental OEM costs per unit CO2 emission reduction, per unit user cost reduction and per unit total powertrain cost reduction over the vehicle lifetime.

5. A detailed investigation of different market scenarios, in terms of fuel price, battery life duration and battery cost, and of their effects on the identification of the optimal design, as well as on the performance of the resulting vehicles.

2. Powertrain Design

The design optimization procedure has been applied to three different hybrid architectures in this paper. The first vehicle, whose scheme is reported in Figure 1 (top), is referred to as Torque-Coupling Vehicle (TCV). A single-speed gearbox (GB) has been installed as a torque-coupling device. The electric machine (EM) is connected to the second GB shaft, while the engine and the driveline are connected to the first GB shaft.

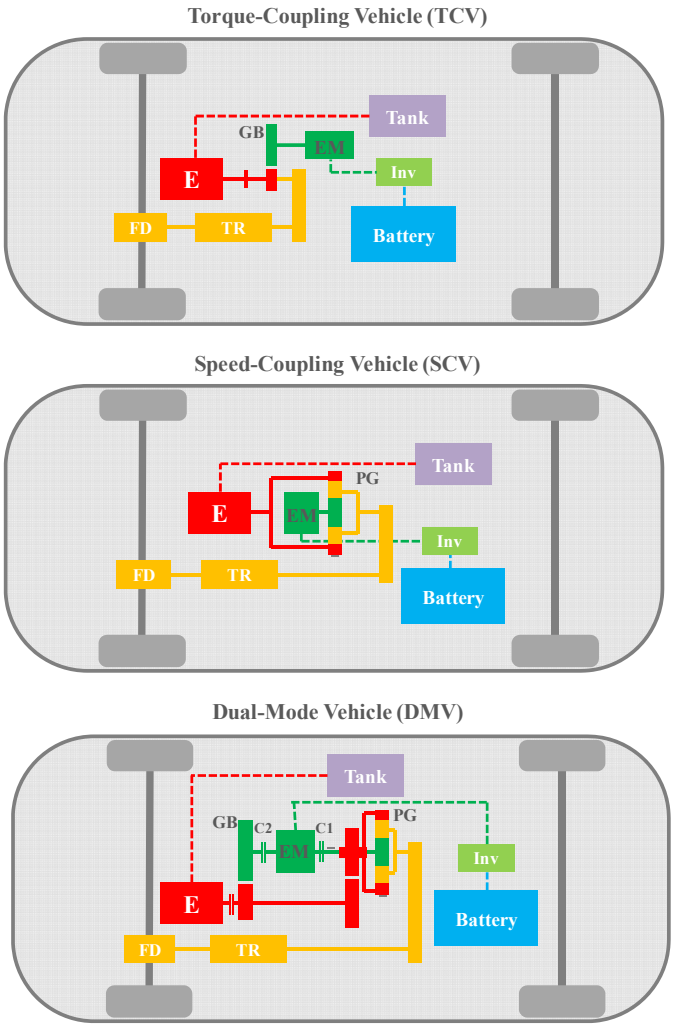

Figure 1 – Scheme of the hybrid electric vehicles.

The second hybrid vehicle (Figure 1, middle) has here been referred to as Speed-Coupling Vehicle (SCV). A planetary gear set (PG) has been installed as a speed-coupling device. The engine is connected to the PG ring, the EM is connected to the PG sun, and the driveline is connected to the PG carrier.

The third hybrid vehicle (Figure 1, bottom) is a newly proposed architecture, which includes SC and TC devices at the same time, and has here been referred to as a Dual-Mode Vehicle (DMV). A planetary gear set and a gearbox have been installed as speed-coupling and torque-coupling devices, respectively. The engine (E) is connected to the first GB shaft and to the PG ring, the EM is connected to the second GB shaft and to the PG sun, and the driveline is connected to the PG carrier. Two different clutches have been inserted in order to enable either the speed-coupling mode, if clutch C1 is engaged and clutch C2 is released, or the torque-coupling mode, if clutch C2 is engaged and clutch C1 is released. The two mechanical connections enable the engine operating point to be shifted either horizontally (speed) or vertically (torque).

The driveline is depicted in yellow for each architecture in the figure, and it consists of the transmission (TR) and the final drive (FD). The battery is connected to the electric machine through the inverter (Inv).

3. Vehicle Model

The hybrid electric vehicles investigated in this study have been compared to a reference case, i.e., a conventional vehicle equipped with a compression-ignition engine. The reference vehicle is equipped with a 2.9 L prototype Euro 5 GMPT-E diesel engine (130 kW at 4000 rpm, 356Nm at 1500 rpm). The total vehicle mass is 1536 kg (the chassis mass is 1250 kg), the frontal area A_v is 2 m^2, the drag resistance coefficient c_x is 0.3 and the tire radius is 0.3247 m. The chassis mass, frontal area, drag resistant coefficient and tire radius have been kept constant for the different simulated hybrid vehicles. The performance capability of the vehicles has been measured as a combination of acceleration time, elasticity time and maximum velocity over different uphill roads, in order to estimate the overall performance index (PI). Each hybrid vehicle layout obtained from the optimal vehicle design tool has had to provide a similar performance to that of the reference vehicle.

256 The kinematic vehicle model has been developed in the Matlab environment [27].

257 3.1 Components

258 3.1.1 Engine

259 Two different prototype Euro 5 GM compression ignition engines, with displacements of 1.7 L and 1.3 L,
260 respectively, have been employed in this study. The first engine, which is here referred to as D1, provides a
261 maximum power of 97 kW at 3700 rpm and a maximum torque of 304 Nm at 2400 rpm. The second engine,
262 referred to as D2, provides a maximum power of 70 kW at 4000 rpm and a maximum torque of 206 Nm at 1800
263 rpm. The adoption of different engines is of fundamental importance in order to be able to investigate the impact
264 of the degree of hybridization on the performance of the hybrid vehicle.
265 The performance of the engine was modeled using experimentally-derived look-up tables. The mass flow rate of
266 both the fuel and NO_x emissions were evaluated by interpolating a 2D map, which is a function of the engine
267 power and speed. The corresponding CO_2 emissions were linearly determined as follows [26, 28]:

268 $$\dot{m}_{co2} = 2.65 \cdot \frac{\dot{m}_{fc}}{\rho} \quad (1)$$

269 where ρ is the fuel density, $\dot{m}_{fc}$ is the fuel mass flow rate and 2.65 represents a conversion factor. The latter was
270 obtained considering a combustion reaction of diesel oil with air, such as the one presented in [29], and an
271 average composition of the fuel taken from literature data [30].

272 3.1.2 Electric machine

273 The electric machine model simulates power conversion from the electric to mechanical form, and vice-versa,
274 taking into account energy losses by means of efficiency maps, which are functions of the machine power and
275 speed. The electric machines that have been considered in the present study belong to the brushless permanent
276 magnet electric motor/generator family, and all the data were taken from the official UQM Technologies website
277 [31].

3.1.3 Battery

Lithium-ion batteries have been adopted in this study as the secondary power storage device. The battery model is represented by an equivalent resistance circuit, in which the resistance and the open-circuit voltage of the battery are SOC-dependent. The SOC represents the electrical status of the battery and depends on the equivalent battery capacity C_{bat} and on the flowing current I_{bat}, as follows:

$$SOC = SOC_0 - \int \frac{I_{bat}}{C_{bat}} \cdot dt \quad (2)$$

The battery SOC was limited within the $[0.4 - 0.8]$ range, while the maximum current that may be transferred through a cell was established as 120A.

A phenomenological damage accumulation model, based on the "accumulated Ah-throughput" concept has been adopted to estimate the depletion of the battery life. The λ parameter, which represents the effective Ah-throughput, can be computed as follows [32]:

$$\lambda = \int \sigma \cdot |I_{bat}| \cdot dt \quad (3)$$

This parameter represents the amount of charge that would have to be exchanged when a nominal cycle is adopted in order to have the same aging effect as the actual cycle the battery has undergone. The severity factor σ represents the relative aging effect, with respect to the nominal cycle, and it is higher than 1 for severe aging conditions (i.e. which would lead to a shorter life). The severity factor is estimated as follows [28, 32]:

$$\sigma = 1.5 \cdot \left(\frac{I_{bat}}{C_{bat}}\right)^2 + 1 \quad (4)$$

The residual battery life λ_r, which represents the fraction of charge that could still flow through the battery before the end of its life, is determined as follows:

$$\lambda_r = 1 - \frac{\lambda}{\Lambda} \quad (5)$$

where Λ is the battery life, which has here been set to 20000 Ah. The end of life condition is defined as the instant at which $\lambda_r = 0$.

3.1.4 Torque-coupling and speed-coupling devices

A single-speed two-shaft gearbox has been used in this study as a mechanical torque-coupling device, as shown in Fig. 1. It has the function of coupling together the torque from the engine and the electric machine and of providing the output torque to the transmission shaft.

A planetary gear unit, which mechanically connects the power derived from all the power sources, has been used as a speed-coupling device. It has the function of coupling the speeds of two different power sources that enter the device separately and of providing the output torque to the transmission shaft. This device consists of three rotating nodes, namely a sun gear, a ring gear and a carrier gear, as shown in Fig. 1, which are linked by a few small pinion gears.

The equations used to derive the input/output torque and speed of the torque-coupling and speed-coupling devices are well known and commonly used in the literature [28] and have not been reported here for the sake of brevity.

3.1.5 Transmission

Table 1 – Transmission speed ratio specifications.

GN	1	2	3	4	5	6
τ [-]	4.17	2.13	1.32	0.95	0.75	0.62

The driveline consists of a 6-speed gearbox (which is referred to as “transmission” in this study) and of the front final drive. The transmission power losses have been estimated by means of an efficiency map, which is a function of the output shaft speed and torque, as well as of the selected gear number. The transmission inertia has also been taken into account. The final drive has instead been modeled as a torque multiplier, while power losses and inertia contributions have been neglected. The transmission speed ratio values are reported in Table 1 for each gear.

3.2 Determination of the power and speed of the engine and electric machine

The total vehicle power demand P_v at the wheel level is the sum of several contributions: the rolling resistance, the grade resistance, the drag resistance and the inertia. The total power demand of the vehicle can be expressed as follows:

$$P_v = \left(m_v \cdot g \cdot r_v \cdot \cos(\alpha_r) + m_v \cdot g \cdot \sin(\alpha_r) + \frac{1}{2}\rho_{air} \cdot c_x \cdot A_v \cdot {V_v}^2 + \left(m_v + \frac{I_{wh}}{R_{wh}}\right) \cdot \dot{V}_v\right) \cdot V_v \quad (6)$$

where m_v is the vehicle mass, g is the gravitational acceleration, r_v is the rolling resistance coefficient of the vehicle, α_r is the slope of the road, V_v is the vehicle velocity, A_v is the front area of the vehicle, ρ_{air} is the air density, c_x is the aerodynamic drag coefficient, R_{wh} is the dynamic wheel radius and I_{wh} is the wheel inertia. The working condition of the vehicle may be either of a traction type, if the power is positive, or of a braking type, if the power is negative. The power at the final drive level is therefore determined as follows:

$$P_{fd} = \begin{cases} P_v, & traction \\ \gamma_{fr} \cdot (1 - \gamma_{br}) \cdot P_v, & braking \end{cases} \quad (7)$$

where the γ_{fr} factor represents the power split between the front and the rear wheels of the vehicle during the braking phase, while γ_{br} represents the power share that has to be managed by the mechanical frictional brakes during braking. The γ_{fr} value has been kept constant and equal to 0.75 for all of the simulations, while the value of γ_{br} has been set at 0.1.

The power required at the front powertrain level is obtained as follows:

$$P_f = \left(P_{fd} + P_{tr,in}\right) \cdot {\eta_{tr}}^k + P_{e,in} + P_{em,in} \quad (8)$$

where $P_{tr,in}$, $P_{e,in}$ and $P_{em,in}$ are the inertial power of the transmission, of the engine and of the electric machine, respectively, η_{tr} is the transmission efficiency, and exponent k is equal to 1, if the vehicle is braking, or equal to -1 otherwise.

The angular velocity ω_f at the front powertrain level is a function of the control variable τ as follows:

$$\omega_f = \tau \cdot \tau_{fd} \cdot \frac{V_v}{R_{wh}} \quad (9)$$

where τ_{fd} is the speed ratio of the final drive.

The formulation used to determine the power of the engine P_e and of the electric machine P_{em} is obtained considering the value of the sub-control variable α:

$$P_e = (1 - \alpha) \cdot P_f \quad (10)$$

$$P_{em} = \alpha \cdot P_f \quad (11)$$

As far as the formulation of the speed of the engine and of the electric machine is concerned, two different modes have to be considered.

Mode 1 – torque coupling

The engine speed, with reference to the Willis method applied to a planetary gear set [28], is obtained if the sun shaft is blocked:

$$\omega_{e,t} = \frac{1+\tau_{sc}}{\tau_{sc}} \cdot \omega_f \quad (12)$$

where $\omega_{e,t}$ and ω_f are the speed of the engine and of the front powertrain, while τ_{sc} is the PG speed ratio. The electric machine is now connected to the second GB shaft, and its speed can be defined as follows:

$$\omega_{em,t} = \tau_{tc} \frac{1+\tau_{sc}}{\tau_{sc}} \cdot \omega_f \quad (13)$$

where $\omega_{em,t}$ is the speed of the electric machine and τ_{tc} is the GB speed ratio.

Mode 2 – speed coupling

The engine power, with reference to the torque correlations for the three shafts of the planetary gear set [28], can be expressed as follows:

$$P_e = (1 - \alpha) \cdot P_f = (1 - \alpha) \cdot T_f \cdot \omega_f = (1 - \alpha) \cdot \frac{1+\tau_{sc}}{\tau_{sc}} \cdot T_e \cdot \omega_f = T_e \cdot \omega_e \quad (14)$$

where T_e and T_f are the torque at the engine and at the front powertrain level, respectively, while ω_e and ω_f are the speed of the engine and of the front powertrain, and τ_{sc} is the PG speed ratio. The engine speed is therefore obtained as:

$$\omega_{e,s} = (1 - \alpha) \cdot \frac{1+\tau_{sc}}{\tau_{sc}} \cdot \omega_f \quad (15)$$

In a similar way, the power of the electric machine can be written as follows:

$$P_{em} = \alpha \cdot P_f = \alpha \cdot T_f \cdot \omega_f = \alpha \cdot (1 + \tau_{sc}) \cdot T_{em} \cdot \omega_f = T_{em} \cdot \omega_{em} \quad (16)$$

where T_{em}, ω_{em} are the torque and the speed of the electric machine, whose speed is calculated as follows:

$$\omega_{em,s} = \alpha \cdot (1 + \tau_{sc}) \cdot \omega_f \quad (17)$$

The aforementioned equations describe the vehicle model for DMVs. The TCV model equations can be obtained from the DMV model if the speed ratio $\tau_{sc} \to \infty$. The SCV model equations can instead be obtained from those of the DMV, if the speed ratio τ_{tc} is set at 1.

3.3 Control/state variables and their discretization

The gear number, GN, and the power flow, PF, have been chosen as the control variables in this study. The GN variable determines the speed ratio of the transmission, τ (see Table 1). The GN domain is defined by the $S_{gn} = \{1, 2, \cdots, 6\}$ set, since a 6-speed transmission has been adopted on the front axle. The PF variable is related to the management of the power of the engine and of the electric machine. In particular, it controls the sub-control variable α, which quantifies the power contribution provided by the battery through the front axle, with respect to the front vehicle power demand (see Eqs. (10-11)). The PF domain is defined by the $S_{pf} = \{1, 2, \cdots, N_{pf}\}$ set, where N_{pf} stands for the number of different power flow types. The default size of S_{pf} has been set equal to 4 for the TCV and SCV architectures and to 7 for DMV.

All the different values of the PF control variable are listed in Table 2, where **pe** stands for pure electric mode, **pt** for pure thermal mode, **ps** for power split mode and **bc** for battery charge mode, while **tc** stands for torque-coupling and **sc** for speed-coupling.

Two different pure-electric modes are possible for the dual-mode vehicle: the electric machine can in fact drive the vehicle either in torque-coupling mode (**pe.tc**) or in speed-coupling mode (**pe.sc**). Its speed is expressed either by Eq. (17) or by Eq. (13), according to which mode is selected, while engine speed is null. Only one pure-thermal mode, in which both the electric machine clutches are disengaged and the engine is connected to the driveline in the torque-coupling mode, is possible for this vehicle powertrain.

Table 2 – Working modes of the TCV, SCV and DMV architectures.

PF	**1**	**2**	**3**	**4**	**5**	**6**	**7**	
description	pe.tc	pe.sc	pt.tc	ps.tc	bc.tc	ps.sc	bc.sc	
α	1	1	0	½	-½	½	-½	N_{pf}

TCV	✓		✓	✓	✓			**4**
SCV		✓	✓			✓	✓	**4**
DMV	✓	✓	✓	✓	✓	✓	✓	**7**

Finally, the electric machine can work either to assist the engine or to charge the battery, and it can be connected either in speed-coupling mode or in torque-coupling mode. The power of each component is identified according to the value of the sub-control variable α (see Eqs. (10-11)). The speeds of the engine and of the electric machine are obtained by means of Eq. (15) and Eq. (17), respectively, if the speed-coupling mode is enabled, otherwise by means of Eq. (12) and Eq. (13), respectively, if the torque-coupling mode is selected.

A set of constraints has been introduced in order to identify the feasible combinations of the GN and PF control variables at each time instant, according to the vehicle driving conditions.

With reference to the state variables, the state of the engine, which can be equal to 0 if the engine is off, or equal to 1 otherwise (the related discrete set is therefore $S_{es} = \{0, 1\}$), was chosen as the first variable. The battery SOC was chosen as the second state variable. It can vary in the $S_{soc} = \{0.4, 0.4001, \cdots, 0.8\}$ discrete set, since 4000 discretization steps have been considered. While the evolution of the battery SOC depends on the time-history of the two control variables, the engine state is obtained directly as a function of the instantaneous value of the power flow.

4 Identification of the optimal control strategy

4.1 Objective function

The optimal policy or control strategy $u^*(t)$ is determined by minimizing an objective function, J, while the constraint on the final SOC and NO_x emissions has to be guaranteed. The mathematical formulation of the problem is:

$$u^*(t) = \min_{u(t) \in S^*(t)} J(u(t)) \tag{18}$$

$$SOC_{end} \geq SOC_0 \tag{19}$$

$$M_{nox} \leq M_{nox,ds} \quad (20)$$

where u(t) is the generic policy or control strategy and $S^*(t)$ is the set of feasible combinations of control variables for each time interval t. SOC_{end} is the battery SOC at the end of the mission, SOC_0 is its initial value, M_{nox} is the cumulated NO_x emission mass of the hybrid vehicle at the end of the mission and $M_{nox,ds}$ is the cumulated NO_x emission mass of the conventional reference vehicle equipped with the same downsized engine as that of the hybrid vehicle. $S^*(t)$ is a subset of all the combinations of the control variables.

The battery SOC at the end of the mission has to be higher or equal to that at the beginning, as the architecture is of the non-plug-in type.

If the after-treatment devices are not sufficient to meet the emission limits, the engine-out NO_x levels could be controlled directly by means of the control strategy. Similarly, the cost related to battery life depletion might become extremely significant if a control strategy optimization is completely oriented toward a reduction in fuel consumption. The objective function J has therefore been defined to include not only fuel consumption, but also NOx emissions and battery aging effects, as follows:

$$J = \alpha_1 \frac{FC}{FC_{rv}} + \alpha_2 \frac{M_{nox}}{M_{nox,ds}} + \alpha_3 \frac{BP}{FP \cdot FC_{rv}} \cdot \frac{\lambda}{\Lambda} \quad (21)$$

where FC is the cumulated mass of fuel consumed over the mission (kg), FC_{rv} is the cumulated mass of fuel consumed by the reference vehicle (kg), BP is the cost related to battery replacement ($), FP is the fuel price ($/kg), λ is the effective battery life consumption (Ah) and Λ is the battery life (Ah). Three weighting factors have been introduced, namely α_1, α_2 and α_3, in order to adjust the relative importance of the related terms. This formulation allows the fuel consumption, the NO_x emissions and the battery life depletion effects to be taken into account at the same time.

Whenever the NO_x emissions are not taken directly into account in the optimization process, Eq. (20) still has to be satisfied.

4.2 Dynamic programming

A fast running dynamic programming (DP) algorithm has been developed and implemented in the vehicle design tool in order to identify the control strategy.

Several computational techniques were introduced in order to reduce the simulation time as much as possible. One of these techniques is based on the splitting of the vehicle model evaluations and of the DP-based optimization stage. The model evaluations are pre-processed a-priori for all the possible combinations of the control variables of the problem and the results of the simulations are indexed. In this way, the DP-based algorithm can rely on pre-calculated data to extract the optimal policy, instead of continuously running the vehicle model, which is the main cause of the high computational time [26].

Furthermore, the state grid that has to be generated for the battery SOC has also been exploited for other state variables (such as the NOx emissions), in order to manage multiple constraints of the optimization problem, such as those expressed in Eq. (19) and Eq. (20).

A third technique has been adopted in order to simulate the vehicle performance over a more sparse time grid, without compromising the accuracy of the result. In the present study, the time domain has been discretized uniformly with a time step of 3 s in order to create the corresponding time grid of equispaced intervals.

This algorithm allows all the different vehicle designs to be compared on an equal basis, while rule-based tools may promote some designs because of biasing tuned rules. Specific vehicle control units can be developed in the subsequent step, when the design has been obtained and the DP-algorithm has established the vehicle design benchmark.

5 Optimal vehicle design

The tool that has been used to identify the optimal design of each hybrid vehicle is a refined version of that shown in [25, 26]. Basically, the tool is based on the generation of a large number of different layouts (in terms of engine size, electric machine size and speed ratios of the TC/SC devices and of the final drive) for each vehicle architecture. A preliminary selection of the feasible layouts was carried out, considering performance and emission constraints. The optimal control strategy was then identified for each feasible layout and the overall powertrain cost was then calculated. The latter includes the production costs and the operating costs related to fuel consumption and to battery life depletion. Finally, the layouts that led to the minimum powertrain cost were selected as optimal.

5.1 Cost definition

The optimal layout x^* has been selected for each hybrid vehicle architecture by minimizing the total powertrain cost C_{pt}. The identified layout must guarantee specific performance and emission constraints. The mathematical formulation of the problem is defined as follows:

$$x^* = \min_{x \in X^*} C_{pt}(x) \tag{22}$$

$$PI(x) \leq PI_{rv} \quad PI_e(x) \leq 1.4 \cdot PI_{rv} \quad AER(x) \geq 2.5\ \text{km} \quad M_{nox}(x, y) \leq M_{nox,ds}(y) \tag{23}$$

where x is the vector that contains the parameters that univocally define the layout of each vehicle, x^* is the optimal layout, PI(x) and $PI_e(x)$ represent the performance index of the hybrid vehicle, whose design is defined by x itself, in hybrid mode and in pure-thermal mode, respectively, PI_{rv} is the performance index of the reference vehicle (see Eq. (37)), AER, namely the all-electric range, represents the distance that the vehicle has to cover in pure electric mode, using 60% of the battery energy content, $M_{nox}(x, y)$ is the cumulated nitrogen oxide mass emission of the hybrid vehicle with the x layout over the y mission, while $M_{nox,ds}(y)$ is the cumulated nitrogen oxide mass emission of the reference vehicle equipped with the same downsized hybrid vehicle engine over the same mission y.

The X^* set contains a large number of layouts that have been found to be feasible over several driving missions. The total powertrain cost C_{pt} may be defined in several ways, according to the specific requirements and/or targets of the design procedure. In this study, six different definitions have been taken into account:

1. ***Production*** (C_{pr}): the cost of the powertrain components.
2. ***OEM*** (C_{oem}): the cost that the OEM has to deal with. It consists of the production costs and a fraction of the costs due to battery replacement. It has been speculated that the OEM might be interested in partially financing the purchase of additional batteries, if they are required over the lifetime of the vehicle. This is a reasonable policy that could be adopted by the OEM in order to promote the introduction of hybrid vehicles onto the market.
3. ***Fuel*** (C_{fc}): the cost of the fuel required to drive the vehicle.
4. ***Operating*** (C_{op}): the fuel cost and the cost due to any battery replacement.

5. ***User*** (C_{usr}): the cost concerning the user, i.e. the fuel cost and a fraction of the battery replacement costs (this is basically an operating cost-oriented definition, as it does not include the cost required to purchase the vehicle and the costs related to insurance/taxes).
6. ***Total*** (C_{tot}): the sum of the production cost and the operating cost.

The production cost C_{prod} takes into account the cost of the engine C_e, of all the electric machines C_{em} and of the battery pack C_{bat}:

$$C_{prod}(x) = C_e + C_{em} + C_{bat} \quad (24)$$

which can be broken up into:

$$C_e(x) = 12 \cdot P_{e,max} + 424 \quad (25)$$

$$C_{em}(x) = 21.7 \cdot P_{em,max} + 425 \quad (26)$$

$$C_{bat}(x) = 350 \cdot E_{bat,tot} + 680 \quad (27)$$

where $P_{e,max}$ is the maximum engine power [kW], $P_{em,max}$ is the maximum power of the electric machine [kW] and $E_{bat,tot}$ is the energy content of the battery [kWh]. The method used to estimate the cost of the components was derived from [33], but the battery cost has been updated, considering more recent data [34].

As far as the operating cost evaluation is concerned, it is first necessary to evaluate the fuel consumption and the battery life over a given driving mission. These quantities depend on the control strategy to a great extent.

The minimum achievable fuel cost C_{fc}^* is then estimated as follows:

$$C_{fc}(x, u) = \frac{FP \cdot D \cdot I}{\rho \cdot N \cdot d} \cdot FC(u^*) \quad (28)$$

where FP is the fuel price ($/kg), D = 250000 km is a reasonable distance covered by the vehicle during its lifetime, N = 10 represents the time horizon (year), d is the distance of the specific mission the vehicle is trained over. FC is the cumulated fuel consumption mass (kg), while u^* is the optimal policy obtained with DP that minimizes the objective function J, defined in Eq. (21), over that vehicle mission. The I term is related to the inflation phenomena and is estimated as follows:

$$I = \sum_{j=1}^{N} (1 + i)^j \quad (29)$$

where i is the inflation index.

The cost related to the battery replacement requires the calculation of the number of batteries that have to be employed during the life of the vehicle. To this aim, the battery usage BU has been introduced as follows:

$$BU = \frac{\lambda}{\Lambda} \cdot \frac{D}{d} \tag{30}$$

where λ is the effective life consumption of the battery (Ah) and Λ is the battery life (Ah).

The battery replacement cost C'_{br} has been calculated as follows:

$$C'_{br} = C_{bat} \cdot \frac{I}{N} \cdot (BU - 1) \tag{31}$$

However, since the first battery is part of the initial vehicle, it has not been included in the operating costs. A second definition has therefore been taken into account:

$$C_{br} = \max\left(0, C_{bat} \cdot \frac{I}{N} \cdot (BU - 1)\right) \tag{32}$$

The OEM costs have instead been estimated as follows:

$$C_{oem} = C_{pr} + C_{br}/2 \tag{33}$$

while the user cost has been estimated as:

$$C_{usr} = C_{fc} + \min\left(C'_{br}, C_{br}/2\right) \tag{34}$$

The operating costs have been defined as follows:

$$C_{op} = C_{fc} + C_{br} \tag{35}$$

Finally, the total costs are the sum of the three terms, namely the production, the fuel consumption and battery replacement costs:

$$C_{tot} = C_{pr} + C_{fc} + C_{br} \tag{36}$$

5.2 Vehicle performance constraint

The performance index of each vehicle has been estimated taking into account:

1. The time necessary to cover 1 km at the maximum velocity of the vehicle $V_{v,max}(\alpha)$ over five uphill climbing roads with different slopes α.
2. The response time to increase the velocity over a flat road, starting from three different initial speeds.

The formulation is:

$$PI(x) = \sum_{\alpha} \frac{3600}{V_{v,max}(\alpha)} + t_{0-100} + t_{60-100} + t_{80-120} \quad (37)$$

where t_{0-100} is the 0-100 km/h acceleration time (free gear shift strategy), t_{60-100} is the 60-100 km/h acceleration time (5th gear fixed) and t_{80-120} is the 80-120 km/h acceleration time (6th gear fixed). The maximum velocity of the vehicle has been estimated over each uphill road using the following formulation:

$$V_{v,max}(\alpha) \geq V_v | P_{pt}(V_v) = P_v(V_v, \alpha) \quad (38)$$

where $P_v(V_v, \alpha)$ is the resistance power of the vehicle necessary to climb a road with slope α at velocity V_v and $P_{pt}(V_v)$ is the maximum power that the powertrain is able to provide at that velocity.

The acceleration time has been estimated with reference to the following:

$$\dot{V}_v = \frac{P_{pt}(V_v) - P_v(V_v)}{m_{v,eq} \cdot V_v} \quad (39)$$

where the equivalent vehicle mass $m_{v,eq}$ also takes into account the inertial power contributions of each component that is involved in accelerating the vehicle itself.

5.3 Toolbox

Figure 2 reports the functional scheme of the bi-level toolbox that has been developed in order to identify the optimal layout of each hybrid vehicle. Each colored bar represents a specific phase of the optimization process. Six different vehicle types (namely, TCV, SCV and DMV combined with the two engines D1 and D2) have been considered in this study (outer green bar in Fig. 2). The tool initially generates a set of different layouts for each vehicle type (light cyan bar in Fig. 2). A generic layout is referred to as x, which is an array that stores the information related to the maximum engine power, maximum electric machine power and the speed ratio of the TC device (for the TCV and DMV), of the SC device (for the SCV and DMV) and of the final drive (FD). The generic x layout is shown at the top of Fig. 2.

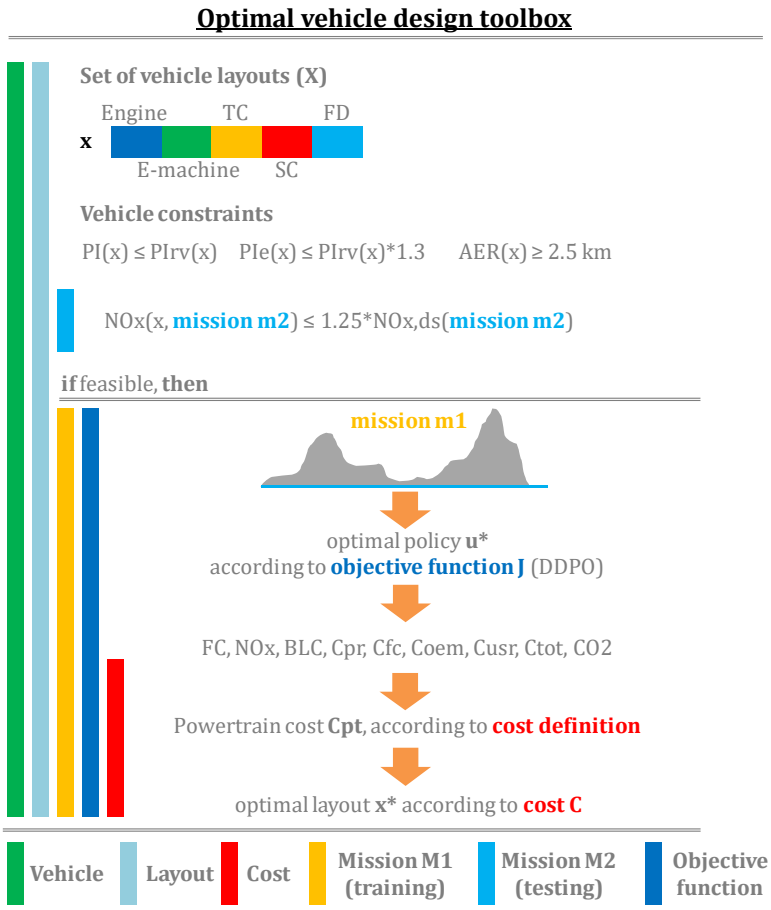

Figure 2 – Scheme of the Optimal vehicle design toolbox.

The vehicle performance of the x layout is then estimated in terms of performance index (PI) and all-electric range (AER) (see section 5.1 for more details) and the NO_x emissions are calculated over the M2 set (cyan bar in Fig. 2) of the test missions (TM1, TM2, TM3, AUDC and AMDC in this study). If all the constraints are satisfied, the layout is marked as feasible.

The optimal policy is then elaborated by means of DP for each feasible layout over each m1 mission of the M1 set (yellow bar in Fig. 2) of the training missions (TM1, TM2, TM3 in this study) using objective function J (FC-BLC-oriented, see Eq. (21)).This phase is represented by the blue bar in Fig. 2. The main outcomes of the different layouts, namely the fuel consumption (FC), the NOx emissions and the battery life consumption are then derived using the optimal policy u^* that was identified in the previous step. The powertrain cost C_{pt} is

obtained according to a given cost definition C (red bar in Fig. 2, see Section 5.1 for the cost definitions), and the optimal layout x^* is then identified for the given cost definition.

In short, the toolbox first evaluates the set of feasible layouts for each vehicle architecture on the test missions, and then evaluates the powertrain costs, adopting a fast-running DP-based algorithm to identify the optimal control strategy over the training missions.

A set of 30k layouts have been generated in this study for the DMV architecture, while a much smaller set (5k) has been generated for the TCV and SCV ones. Since the former architecture is equipped with two mechanical coupling devices, the design domain is much larger. The toolbox then estimates the performance and the NOx emissions for each layout over the M2 set of missions, using a pure-thermal strategy, with the aim of identifying the feasible layouts that satisfy the constraints expressed by Eq. (23). The total number of simulations that are necessary to estimate NOx emissions over the M2 set is $(30 + 5 + 5) \cdot 1000 \cdot 5 \approx 200\text{k}$ (40000 layouts x 5 missions). In addition, $(30 + 5 + 5) \cdot 1000 \approx 40\text{k}$ simulations are required to test the capability of the vehicle, in terms of maximum vehicle velocity and acceleration, with respect to the reference vehicle. This procedure requires a computational time of about 1 h, if several Matlab servers are run on a computer that features an Intel i7 processor (8 CPUs at 2.8 GHz) and 16 GB of RAM. This first stage is of fundamental importance to reduce the number of layouts that have to be investigated in the subsequent stage. This stage (yellow bar in Fig. 2), which in fact computes the optimal control strategy, is much more time consuming than the first stage. It has been found that the number of feasible layouts is of the order of 200, 100 and 1000 for the TCV, SCV and DMV architectures, respectively (starting from original domains of 5k, 5k and 30k layouts). The total number of simulations that has to be carried out in the control strategy optimization phase is therefore $(200 + 100 + 1000) \cdot 3 \cdot 3 \cdot 6 \approx 70\text{k}$, since three training missions, three objective functions and six powertrain cost definitions have been considered. This procedure requires an overall computational time of about 40 h, which can be considered low, compared to the total number of simulations that have to be carried out. A great advantage, in terms of computational time (but also memory demand) reduction, has been obtained using a specific numerical accelerator technique, which shifts the evaluation of the vehicle model to the pre-processing stage. Moreover, since each simulation task is not only fast, but also light, in terms of CPU and memory usage,

several Matlab servers can be launched simultaneously. Another advantage, in terms of computational time reduction, is obtained from the time grid discretization, which allows a large time step (3s) to be used, while maintaining at the same time a good accuracy in the results.

6. Model validation and driving mission specifications

6.1 Validation of the vehicle model

The models of the different components, i.e., the engine, the electric machine and the battery, were assessed by means of experimental tests carried out on a diesel mild hybrid powertrain, equipped with a belt-alternator starter, installed at the dynamic test bed of the ICEAL-PT (Internal Combustion Engine Advanced Laboratory, Dipartimento Energia, Politecnico di Torino). The model was validated by comparing the predicted and experimental fuel consumption and NOx emission values over NEDC for warm and cold start operations. It was found that the inaccuracy resulted to be within ±1 % for the fuel consumption and ±6 % for the cumulated NOx emissions.

For further details on the test rig specifications, the reader can refer to [35], and for further details on the assessment of the model, the reader can refer to [36, 37].

6.2 Specifications of the considered driving missions

The performance of the hybrid vehicles analyzed in this study has been evaluated over a set of five driving missions. The main specifications of the driving cycles are shown in Table 3, which reports the duration T, the covered distance D, the global average velocity $\overline{V}_v$, the effective average velocity $\overline{V}_v'$, the maximum velocity $V_{v,max}$, the maximum vehicle powers $P_{tr,max}$ and $P_{br,max}$ for the traction and braking stages, respectively, the average vehicle powers $\overline{P}_{tr}$ and $\overline{P}_{br}$, as well as the total energy demands E_{tr} and E_{br} for the traction and braking stages. Figure 3 reports the coordinates of each driving mission, where the x-axis indicates the average speed, while the y-axis represents the ratio of the traction/braking energy demand to the covered distance. The dots that lie in the positive quadrant refer to traction, while those in the negative part refer to braking. This picture

provides useful information to help understanding which driving missions are more demanding in terms of energy and velocity.

TM1 has been developed to simulate the vehicle in a mountain-like scenario, TM2 to simulate highway-like conditions over different road slopes, while TM3 has been built in order to include an extensive variation of driving conditions extracted from several homologation cycles.

Table 3 – Main specifications of the set of driving cycles.

	TM1	TM2	TM3	AUDC	AMDC
T [min]	96	108	171	993	1068
D [km]	0.72	2.67	2.76	4.86	29.53
$\overline{V}_v$ [km/h]	27	89	58	17.6	99.5
$\overline{V}_v'$ [km/h]	27	89	58	22.5	100.7
$V_{v,max}$ [km/h]	50	140	108.4	57.2	148.3
$P_{tr,max}$ [kW]	33	51.7	40.5	27	49.3
$P_{br,max}$ [kW]	-48	-100	-51.5	-40.4	-81.5
$\overline{P}_{tr}$ [kW]	15.6	28.7	11.6	6.7	20.6
$\overline{P}_{br}$ [kW]	-15.8	-46.2	-11.1	-4.5	-13.1
E_{tr} [kWh]	0.31	0.72	0.4	0.74	5.01
E_{br} [kWh]	-0.11	-0.23	-0.15	-0.48	-0.67

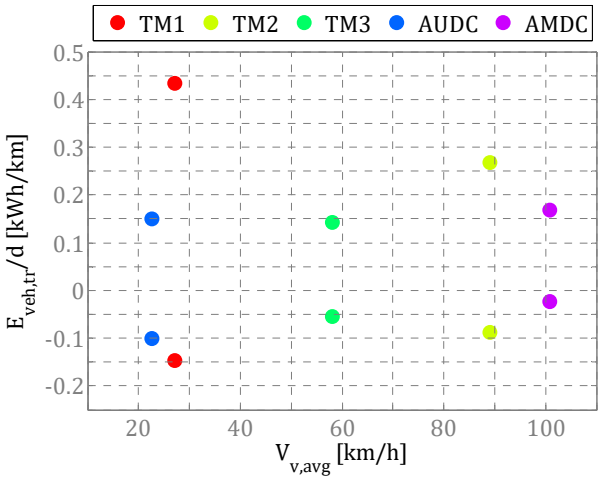

Figure 3 – Traction/braking energy demand, with respect to the covered distance, and average velocity

626 **for the set of driving cycles.**

627 7. Results and Discussion

628 A summary of this section is reported hereafter. Section 7.1 reports the main results obtained from the toolbox
629 application to the vehicle design optimization proposed in this study. Three hybrid vehicles were considered (the
630 speed-coupling architecture, the torque-coupling architecture, and the newly proposed dual-mode architecture),
631 and their performance was compared with that of a conventional reference vehicle, in terms of CO2 emission
632 reduction, NOx reduction and incremental costs. A detailed sensitivity analysis is provided in section 7.2, in
633 order to investigate the impact of the cost definition, of the objective function and of the training driving mission
634 on the optimal design of the vehicle and on its performance with respect to the conventional vehicle. Finally,
635 section 7.3 reports a simulation of different market scenarios, in terms of fuel price, battery life duration and
636 battery cost, and of their effects on the identification of the optimal design, as well as on the performance of the
637 resulting hybrid vehicles.
638 The results are related to simulations in which each mission was repeated in order to cover a total distance of
639 250000 km.

640 7.1 Identification of the optimal layout and analysis of the vehicle

641 performance over different driving missions

642 Table 4 reports the specifications of the layouts of the different vehicles, in terms of maximum engine power,
643 battery and EM power (kW), as well as of the speed ratios of the TC/SC devices and of the final drive, obtained
644 from the application of the toolbox proposed in this study.

645 **Table 4 – Default design of each vehicle, in terms of maximum power of the engine, battery and EM (kW) and**
646 **of the TC, SC and FD speed ratios.**

		Engine power (kW)	Battery power (kW)	EM power (kW)	TC speed ratio	SC speed ratio	FD speed ratio
D1	**TCV**	100	30	30	0.59		3.25

	SCV	100	32.5	32.5		2.7	2.5
	DMV	100	27.5	27.5	0.5	4.5	2.5
D2	**TCV**	70	42.5	42.5	0.91		3.25
	SCV	70	50	50		3	2.5
	DMV	70	40	40	0.5	4.2	2.5

The main specifications of each vehicle, in terms of total mass, performance index (PI), total powertrain cost over the lifetime and payback distance (estimated over the TM3 mission) are instead reported in Fig. 4.

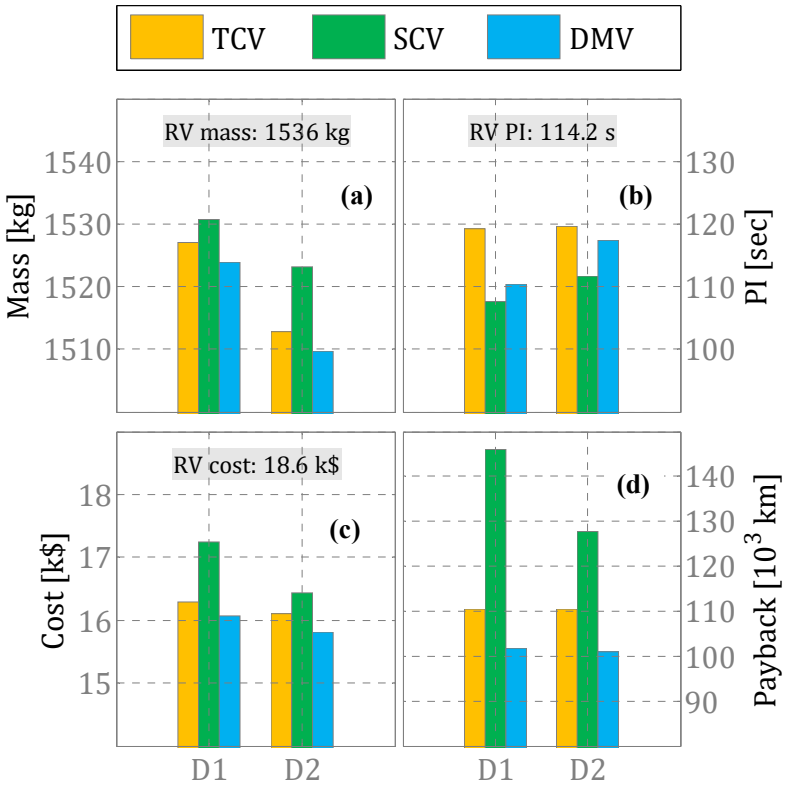

Figure 4 – Main specifications of the default design of each considered hybrid vehicle, estimated over the TM3 mission.

The optimal design of each vehicle has been obtained over the TM3 mission, using the total powertrain costs definition (i.e., Eq. (36)) and the FC-BLC-oriented optimization. These choices are explained in the following subsections.

The total mass of the hybrid vehicles resulted to be the same as that of the conventional vehicle (Fig. 4a) because of the power density of the battery, which is significantly high for non-plug-in hybrid vehicles (i.e., twice the

specific power of a conventional vehicle engine). The SCV, equipped with the D1 engine, was the heaviest, while DMV-D2 was the lightest.

As far as the total costs are concerned (Fig. 4c), the vehicles equipped with the D2 engine are capable of reducing the total costs by 2.5%, compared to the corresponding vehicles equipped with the D1 engine, except for SCV-D2, which shows a reduction of 5%. The maximum cost reduction, with respect to the reference vehicle, is obtained for DMV-D2 (17.7%).

The cost savings also depend on the distance covered by the vehicle over a certain period: the longer the distance, the greater the operating cost reduction. The break-even point represents the distance that each vehicle has to cover to counterbalance the initial investment. A significant result is that the proposed dual-mode vehicle leads to the lowest powertrain costs and to the shortest payback distance.

Figure 5 reports the increase in the OEM cost (first row), as well as the decrease in the user cost (second row), in the CO2 emissions (third row) and in the total costs (fourth row), for the hybrid vehicles with the optimal baseline layout tested over each mission of the M2 set (TM1, TM2, TM3, AUDM, AMDC).

Each black dashed line in the figure shows the average variation in the corresponding quantity over the set of driving cycles for the different vehicles. Each textbox in the chart reports instead the average (left) and the difference between the maximum and minimum values (right) over the five driving cycles. It can be observed that DMV-D1 is the most convenient vehicle in terms of OEM costs, since the average increment over the test missions is 110%. It is worth recalling that the OEM cost consists of the production costs and a fraction of the costs due to battery replacement. The different values of the OEM cost increase over different missions for a given layout reported in Fig. 5 are related to different battery replacement costs. In general, TM1 is the most critical mission in terms of battery usage, due to its severe accelerations over both uphill and downhill roads and due to its short distance, which justifies the highest OEM cost when the hybrid vehicle performance is simulated over that mission.

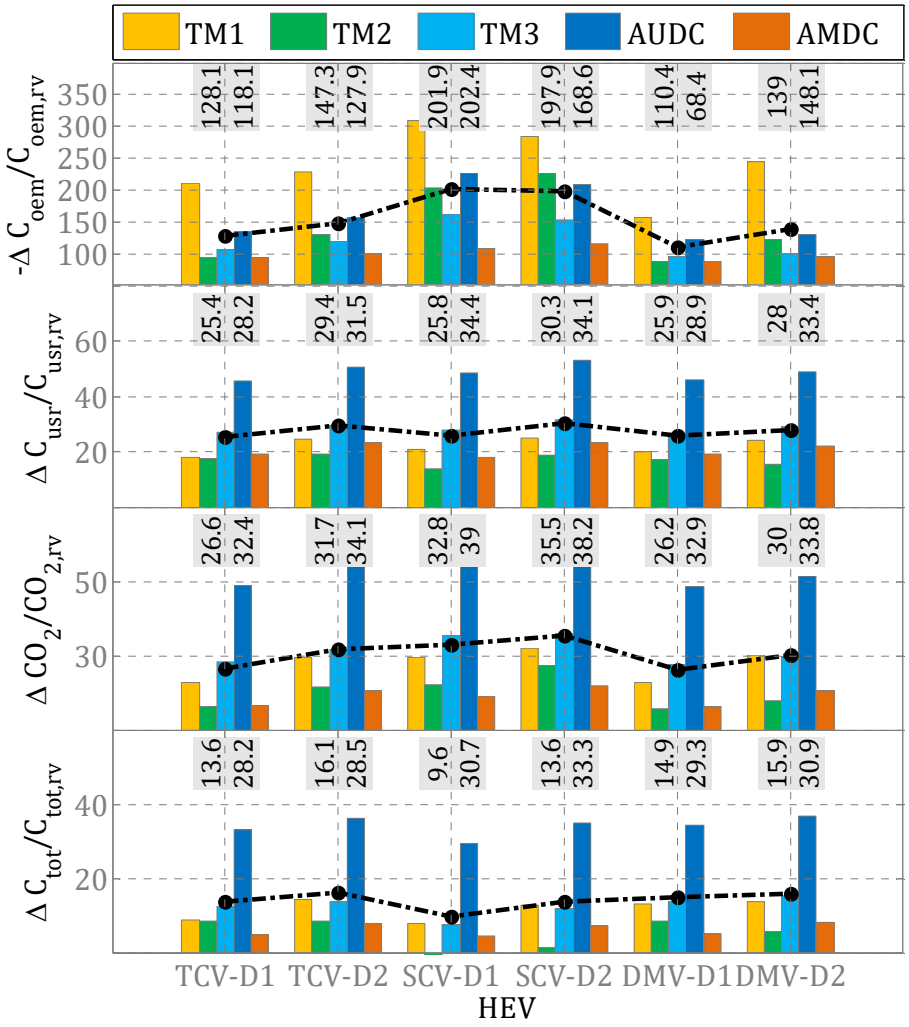

Figure 5 –Increase in OEM costs (first row), user cost reduction (second row), CO2 emissions reduction (third row) and total cost reduction (fourth row), with reference to the reference vehicle, for different test missions and for each vehicle. The optimal layout has been used for each vehicle.

A significant result is that DMV-D1 is the least expensive architecture from an OEM point of view, but its average performance, in terms of user cost reduction and CO2 emission reduction over the vehicle lifetime, is in line with that of the other vehicles. The SCV-D1 leads to the best CO2 emission reduction (32.8%), but this is obtained at the expense of the OEM costs, which are the highest.

In general, the vehicles equipped with the D2 engine outperform the corresponding vehicles equipped with the D1 engine, in terms of user costs, CO2 emissions and total costs. However, they also lead to higher OEM costs,

except for the SCVs, which are characterized by similar OEM costs, regardless of what type of engine is considered.

An additional investigation has been carried out in order to understand which hybrid architectures are the most convenient, considering the testing mission specification and different target functions. The results are reported in Fig. 6. Each point represents a specific driving condition, in terms of average speed (x-axis) and the ratio of the traction energy demand to the covered distance (y-axis). A large set of missions with different specifications was generated for this analysis. The color of each point indicates the best architecture that minimizes the target function over the considered mission. Four different target functions were defined, namely the ratio of the NOx emission reduction to the OEM cost variation (Fig. 6a), the ratio of the CO2 emission variation to the total cost variation (Fig. 6b), the ratio of the CO2 emission variation to the OEM cost variation (Fig. 6c) and the total costs (Fig. 6d). The points corresponding to the TM1, TM2, TM3, AUDC and AMDC missions are also reported.

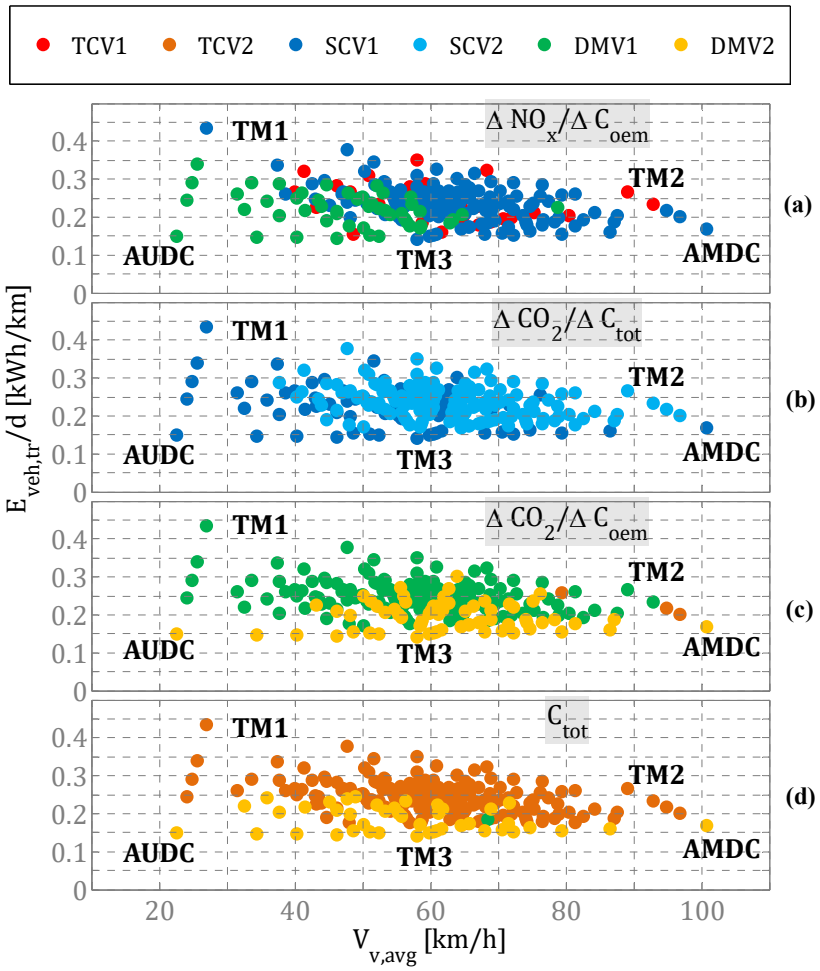

Figure 6 – Optimal hybrid architectures over several driving scenarios, for different target functions.

First, it can be noted, from Fig. 6a, that the best architectures selected to reduce NOx emissions are those equipped with engine D1. This is a consequence of the fact that the D2 engine is smaller than the D1engine, and it generally operates at higher relative load levels, where high NOx emissions occur (the calibration maps of the engines considered in this study were in fact optimized for a conventional vehicle). In order to avoid this issue, a comprehensive optimization tool, which is capable of identifying not only the optimal control strategy of the hybrid powertrains over the mission, but also the optimal values of the main engine parameters (i.e., EGR rate, start of injection), is currently being developed. This tool will incorporate specifically developed low-throughput models that simulate the combustion and emission formation processes in the engine (see [35, 38-40]). The results of this research will be presented in the near future.

Moreover, Fig. 6a indicates that the DMV-D1 is convenient, in terms of NOx emission reduction per unit OEM cost reduction, for driving cycle specifications in the AUDC-TM1-TM3 region, while TCV-D1 is convenient in the TM1-TM3-AMDC-TM2 region. Fig. 6b shows that the speed-coupling architectures lead to the highest potential, in terms of CO2 emission reduction per unit total cost reduction. However, it was found that this result was achieved after an intense exploitation of the battery, which leads to high battery replacement costs (i.e., high OEM and user cost). Fig. 6c shows that SCV is in fact not convenient, in terms of NOx emission reduction per unit OEM cost reduction. In this case, DMVs represent the best choice. The employment of the D1 engine with the smallest battery pack (27.5 kW, see Table 5) is more advisable in the upper region (higher energy demand), while the D2 engine with the largest battery pack (40 kW, Table 5) is advisable in the lower region. Finally, Fig. 6d indicates that DMV-D2 is the best choice, in terms of total powertrain cost, over missions that feature a relatively low specific traction energy demand, while TCV-D2 is better for higher values. It was verified that the total cost reduction for DMV-D2 is mainly due to the reduction in the battery replacement costs, while the TCV-D2 layout shows the best potential to reduce the fuel consumption cost. Missions with a high energy demand, such as TM1 and TM2, favor the choice of TCV-D2, since fuel costs rather than battery replacement costs are the predominant contributions. On the other hand, DMV-D2 is the best choice for driving missions in which battery life depletion is a major concern.

7.2 Sensitivity analyses

Several sensitivity analyses have been carried out, in order to understand the impact of the cost definition (section 7.2.1), of the objective function (section 7.2.2) and of the training mission (section 7.2.3) on the optimal layout and on the performance of the related vehicles.

7.2.1 Impact of the cost definition

The impact of the powertrain cost definition that was used to identify the optimal design (see section 5.1) has been investigated, and the results are shown for each vehicle in Figure 7, which reports the reduction in the OEM cost (Fig. 7a), in the user cost (Fig. 7b), in the CO2 emissions (Fig. 7c) and in the total costs (Fig. 7d), with respect to the reference vehicle, obtained using different architectures (indicated with different colors) and optimized using different cost definitions (indicated by the different groups of bars identified with the acronyms PR, OEM, FC, USR, TOT, i.e., production cost, OEM cost, fuel consumption cost, user cost and total cost, respectively). The results shown in Fig. 7 were obtained using the benchmark optimizer (i.e., DP) and an FC-BLC-oriented optimization over the TM3 training mission. The three weight factors in Eq. (21) were set as follows: $\alpha_1 = 0.5$, $\alpha_2 = 0$, $\alpha_3 = 0.5$.

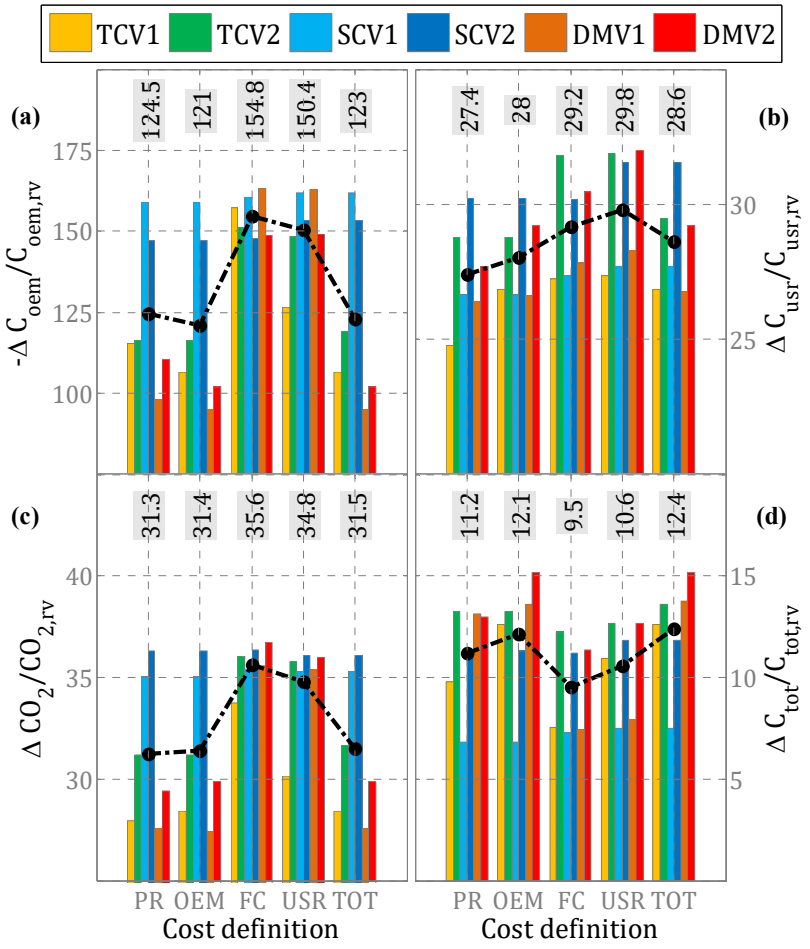

743

744 **Figure 7 – Increase in OEM costs (top left), decrease in user costs (top right), in CO2 emissions (bottom left)**
745 **and in total costs (bottom right), with respect to the reference vehicle, for the different vehicles whose**
746 **layouts have been identified using different powertrain cost definitions (PR, OEM, FC; USR, TOT). The TM3**
747 **mission has been used for training.**

748 Fig. 7a shows that if the user or FC cost definitions are selected for the layout optimization process, the resulting
749 vehicles are characterized by a higher OEM cost increase than the conventional vehicle (about +150%), mainly
750 due to the higher hybridization degree that is required. At the same time, they are capable of providing the best
751 performance, in terms of user cost reduction (29-30%, Fig. 7b) and CO2 emission reduction (about 35%, see Fig.
752 7c). However, they are also penalized in terms of total powertrain cost over the vehicle lifetime (about 10%, see
753 Fig. 7d), mainly as a consequence of the high OEM costs. On the other hand, if the OEM, production or total
754 cost definitions are selected, the resulting vehicles are characterized by a lower OEM cost increase (about +121-

125%, see Fig. 7a) and a higher total cost reduction than the conventional vehicle (11.2-12.4%, see Fig. 7d), but they maintain a good performance in terms of user cost reduction (27.4-28.6%) and CO2 emission reduction (31-32%, see Fig. 7c).

It should be noted that the OEM costs represent a factor of great importance for car manufactures, and they may play a decisive role in promoting a specific vehicle architecture on the market.

The use of the OEM cost definition to identify the optimal layout obviously leads to the lowest OEM cost increase, but at the same time also to reductions in the total costs and in the CO2 emissions, which are of the same order of magnitude as those obtained using the total cost definition.

Table 5 reports the design specifications, in terms of maximum engine, battery and EM power (kW), as well as of the speed ratios of the TC/SC devices and of the final drive of the DMVs, whose layouts were optimized using two different training cycles (TM1 and TM3) and four cost definitions (fuel, operating, OEM and total).

Table 5 – Main specifications of DMVs for two training cycles and four different cost definitions, in terms of maximum power of the engine, battery and EM (kW), and of the TC, SC and FD ratios.

			Engine power (kW)	Battery power (kW)	EM power (kW)	TC speed ratio	SC speed ratio	FD speed ratio
D1	**TM1**	**FC**	100	35	35	2	4.5	2.5
		Oper	100	27.5	27.5	0.5	3.3	2.5
		OEM	100	27.5	27.5	0.5	3.9	2.5
		TOT	100	27.5	27.5	0.5	3.3	2.5
	TM3	**FC**	100	32.5	32.5	2.9	3.9	2.75
		Oper	100	35	35	0.5	3	2.5
		OEM	100	27.5	27.5	0.5	4.2	2.5
		TOT	100	27.5	27.5	0.5	4.5	2.5
D2	**TM1**	**FC**	70	40	40	3.2	2.7	2.5
		Oper	70	50	50	1.4	3	2.5
		OEM	70	42.5	42.5	0.8	3.9	2.75
		TOT	70	42.5	42.5	0.8	3.9	2.75
	TM3	**FC**	70	40	40	2.9	3.3	2.5
		Oper	70	50	50	1.1	3.9	2.5
		OEM	70	40	40	0.5	4.2	2.5
		TOT	70	40	40	0.5	4.2	2.5

It should be noted, in the table, that if the OEM and total cost definitions are used to identify the optimal layout, the maximum power of the electric machine results to be the lowest. It has been verified that this power is the minimum one that allows the vehicle performance constraint to be satisfied, in terms of vehicle longitudinal acceleration. The final drive speed ratio is basically independent of the cost definition. A low TC speed ratio has been chosen when the operating, OEM and total cost definitions have been used (all the definitions take into account battery aging), while higher values (up to 3) are selected if the fuel consumption cost definition is used. The latter definition does not take into account battery aging, and the layout is therefore identified in order to maximize the CO2 emission reduction, regardless of the battery depletion. A low TC speed ratio in fact limits the maximum power of the electric machine in both the regenerative braking and electric traction phases. It has been verified that this determines a limitation of the maximum fraction of recoverable energy during the regenerative braking phases. This in turn leads to a fuel-economy penalization, but at the same time has a positive effect on battery life duration, which depends directly on the energy flux across the battery itself.

The results reported in Fig. 7 have suggested the need to investigate what the ratio would be between the incremental OEM cost of a given hybrid vehicle and the achieved CO2 emission reduction, in order to understand how “expensive” a CO2 emission reduction unit would be in terms of incremental OEM costs. At the same time, the ratio between the incremental OEM cost and the incremental user and total costs, as well as the ratio between the reduction in total costs and the achieved CO2 emission reduction have been investigated. The results related to the DMVs, equipped with the D1 or D2 engines, are reported in Fig. 8 for each cost definition used during the layout optimization process.

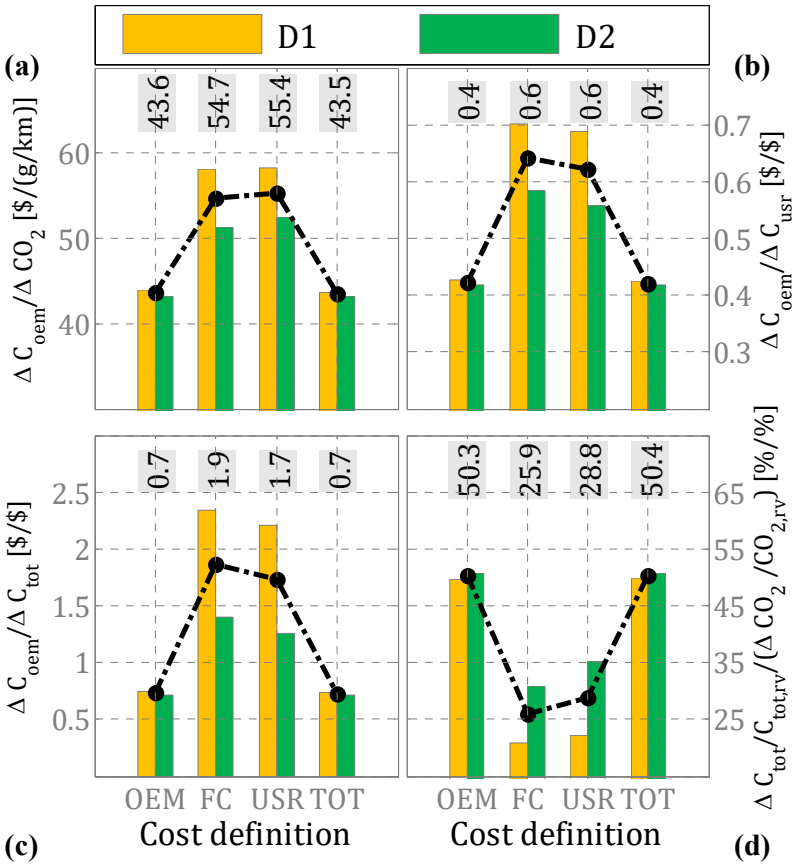

788

789 **Figure 8 – Ratio between the incremental OEM costs and the CO2 emission reduction (a), user cost reduction**
790 **(b) and total cost reduction (c); ratio between the total cost reduction and the CO2 emission reduction (d);**
791 **the DMVs equipped with D1 and D2 engines have been considered.**

792 It can be noted, in Fig. 8a, that the incremental OEM cost necessary to reduce the CO2 emissions by 1 g/km is
793 about $ 43.5, if the optimal layout is identified using the OEM or total cost definitions, while it is about $ 55 in
794 the case when the user or FC cost definitions are adopted. The incremental OEM cost increase per unit user cost
795 reduction (Fig. 8b) follows the same trends as the CO2 emissions (i.e., fuel consumption), and the user costs are
796 closely related to each other. A similar trend can also be observed when the ratio between the incremental OEM
797 cost and the incremental cost is considered (Fig. 8c). In addition, it is worth noting (Fig. 8d) that the ratio
798 between the relative total cost reduction and the relative CO2 reduction is of the order of 50%, if the OEM or the
799 total cost definitions are used to determine the optimal layout, while it is around 26% if the fuel cost or the user

cost definitions are adopted. This means that additional CO2 reductions can be achieved at the expense of higher overall costs, if the layout is optimized on the basis of the fuel cost or user cost definitions.

On the basis of the previous results, the total cost definition can be considered as the best method to identify the optimal layout, as it leads to the lowest incremental OEM costs per unit CO2 emission reduction, per unit user cost reduction and per unit total cost reduction of the hybrid vehicle over its lifetime. However, fuel cost or user cost definitions could also be used to define the optimal layout if a more intense CO2 emission reduction is necessary, regardless of the increment in the powertrain costs. The main reason for the incremental costs related to the adoption of the fuel or user cost definition is related to the fact that a more aggressive use of the electric power unit is realized, and this leads to higher battery replacement costs.

7.2.2 Impact of the objective function

The impact of the objective function on the optimal design and on its performance and costs has been investigated and the results for each vehicle are shown in Fig. 9, which reports the increase in the OEM cost (Fig. 9a), as well as the decrease in the user cost (Fig. 9b), in the CO2 emissions (Fig. 9c) and in the total costs (Fig. 9d). The x-axis reports three different oriented optimizations, namely FC ($\alpha_1 = 1, \alpha_2 = 0, \alpha_3 = 0$ in Eq. (21)), NOx ($\alpha_1 = 0, \alpha_2 = 1, \alpha_3 = 0$) and FC-BLC ($\alpha_1 = 0.5, \alpha_2 = 0, \alpha_3 = 0.5$), which have been used to define the optimal control strategy. The total cost definition was used to identify the optimal layout over the TM3 training mission.

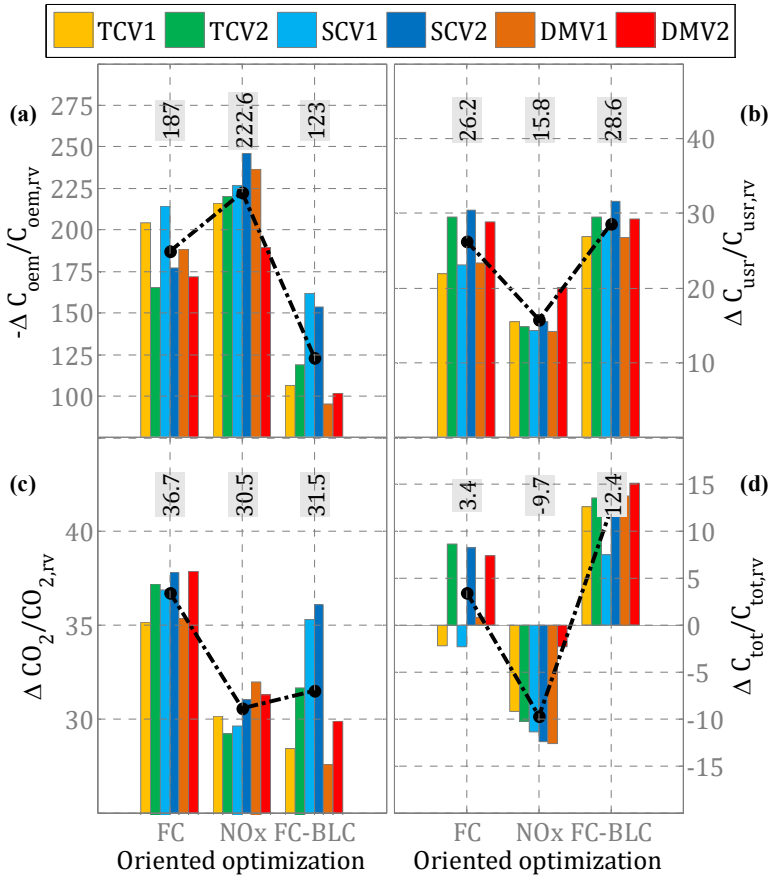

Figure 9 – Increase in OEM costs (top left), decrease in user costs (top right), in CO2 emissions (bottom left) and in total costs (bottom right), with respect to the reference vehicle, for different objective functions and for each type of vehicle. The TM3 mission has been used for layout optimization.

Fig. 9 shows that if the control strategy is identified according to the FC and FC-BLC objective functions, the resulting vehicles show a lower OEM cost increase (Fig. 9a) than the reference vehicle (the FC-BLC function is the best choice from this point of view), a greater user cost reduction (Fig. 9b), a greater CO2 emission reduction (the FC function shows the best potential) and positive total cost reductions (the FC-BLC function leads to the maximum benefit). Since each layout must satisfy the constraints expressed by Eq. (23), which also include an NOx emission limit, the improvements in CO2 emissions and in cost reductions, using the FC- and FC-BLC-oriented optimizations, can be considered consistent.

On the other hand, the adoption of the NOx oriented objective function leads to the highest OEM cost increase (Fig. 9a), to the lowest user cost and CO2 emission reduction (Figs. 9b, c) and to an unacceptable increase in the total powertrain costs over the vehicle lifetime (Fig. 9d).

This occurs because the NOx-oriented objective function is targeted at reducing pollutant emissions as much as possible, regardless of the increase in fuel consumption and battery usage (and in their related operating costs). It has been verified that when the FC-BLC-oriented optimization is adopted, the average NOx emission reduction is 19% and 11% for the hybrid vehicles equipped with the D1 and D2 engines, respectively (results not reported in Fig. 9). Instead, this reduction percentage increases to 47% and 60% when the NOx-oriented optimization is used. However, these promising results are penalized to a great extent by the huge increment in the OEM and total powertrain costs. An NOx emission reduction would in fact imply an intense use of the electric machine and of the battery in both the charging and discharging stages, in order to shift the engine operating conditions to a low NOx emission area, and the battery life would therefore be affected negatively, as would the associated replacement costs.

Finally, it can be noted that if the FC-oriented objective function were adopted instead of the FC-BLC one, an additional Co2 emission reduction decrease of 5% could be achieved, but this reduction would lead to higher OEM and total costs.

The FC-BLC objective function was therefore selected as the best solution, in terms of trade-off between the incremental OEM cost, CO_2 emission reduction and user/total cost reduction, and was adopted to define the optimal layout of the vehicles.

7.2.3 Impact of the training driving mission selection

A sensitivity analysis of the impact of the training driving cycle selected for the optimal layout identification has been carried out in this section.

The performance of the generic x_{m1} layout, which has been optimized over the m_1 training missions of the M1 set (TM1, TM2 or TM3), has been simulated over the m_2 test missions that belong to the M2 set (TM1, TM2, TM3 AMDC and AUDC).

The results are shown in Fig. 10, which reports the increase in OEM cost (Fig. 10a), as well as the reduction in the user cost (Fig. 10b), in the CO2 emissions (Fig. 10c) and in the total costs (Fig. 10d), with respect to the reference vehicle. The i^{th} bar of the j^{th} group represents the average performance of the set of the optimal vehicle layouts over the j^{th} test mission of the M2 set, where each optimal layout was selected over the i^{th} training mission of the M1 set (indicated with different colors). Each black dashed line in the figure and the corresponding number in the text box indicate the greatest difference within each bar block, for different training cycles. The results shown in Fig. 10 were obtained using DP, an FC-BLC-oriented optimization and a total cost definition.

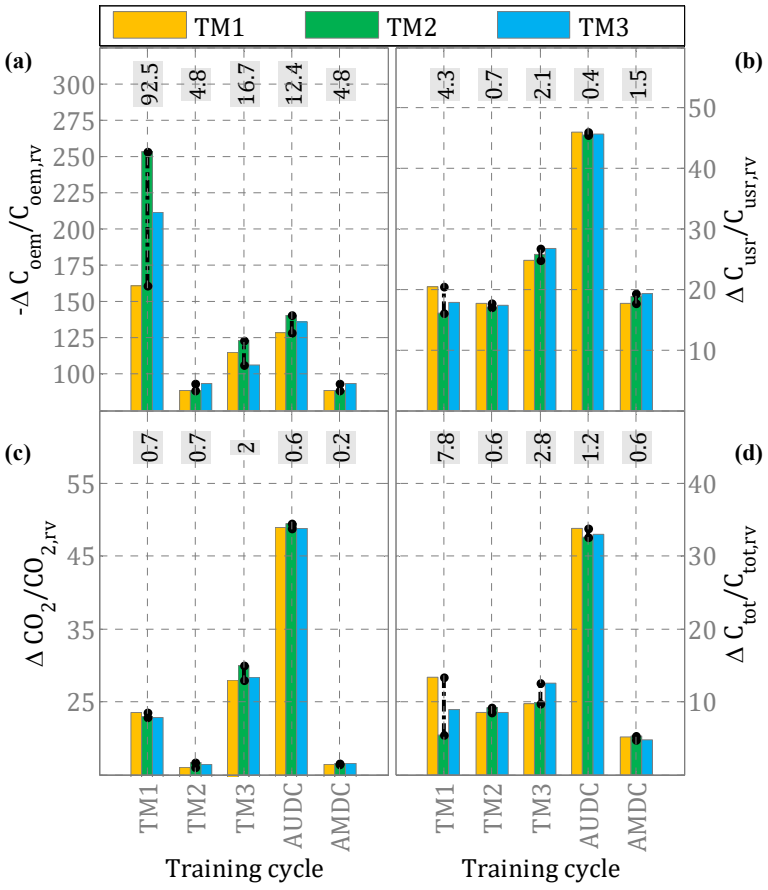

Figure 10 – Increase in OEM costs (a), reduction in user costs (b), in CO2 emissions (c) and in total costs (d), with respect to the reference vehicle, for the different training driving cycles used in the layout optimization process and for each vehicle.

865 It can be noted, in the above figure, that the OEM costs are the terms that are affected the most by the training
866 mission selection. For example, considering a layout that has been defined using either the TM1 mission
867 (mountain-like scenario) or the TM2 driving mission (highway-like scenario), and tested over the TM1 mission
868 (the two cases are indicated with the yellow and green bars in the first group in Fig. 10a), the differences in
869 terms of the OEM cost are significant. Additional costs for the OEM are in fact obtained in this case, while the
870 total costs are less compromised. The performance, in terms of CO2 emission reduction and user cost reduction,
871 is in general affected less by the type of training mission used for the identification of the optimal layout.
872 Finally, it should be noted that the TM3 mission has been designed to include a wide variety of driving
873 conditions extracted from several homologation cycles, and for this reason it was selected as the best candidate
874 for the optimal layout identification.

875 7.3 Analysis of different market scenarios

876 This section reports the results of a detailed investigation of different market scenarios, in terms of fuel price,
877 battery life duration and battery cost, and of their effects on the identification of the optimal design, as well as on
878 the performance of the resulting vehicles.
879 Let us set the current market scenario as the default situation, in terms of fuel cost, battery replacement cost and
880 battery life (case 0). Three additional market scenarios were considered, where the fuel cost increased by 50%
881 over the lifetime of the vehicle (case 1), the battery life increased by 50% (case 2) and the battery cost was
882 halved (case 3).
883 The impact of the different market scenarios on the definition of the optimal layout and on the performance has
884 been investigated, and the results for each vehicle are shown in Fig. 11, which reports the increase in the OEM
885 cost (Fig. 11a), as well as the decrease in the user cost (Fig. 11b), in the CO2 emissions (Fig. 11c) and in the
886 total costs of the powertrain over its lifetime (Fig. 11d), with respect to the reference vehicle. Each black dashed
887 line and the corresponding numbers in the text box indicate the average reduction over the set of vehicles,
888 obtained in different market scenarios. The results shown in Fig. 11 were obtained using the benchmark

optimizer (i.e., DP) and an FC-BLC-oriented optimization. Moreover, the total costs definition was used to identify the optimal layout.

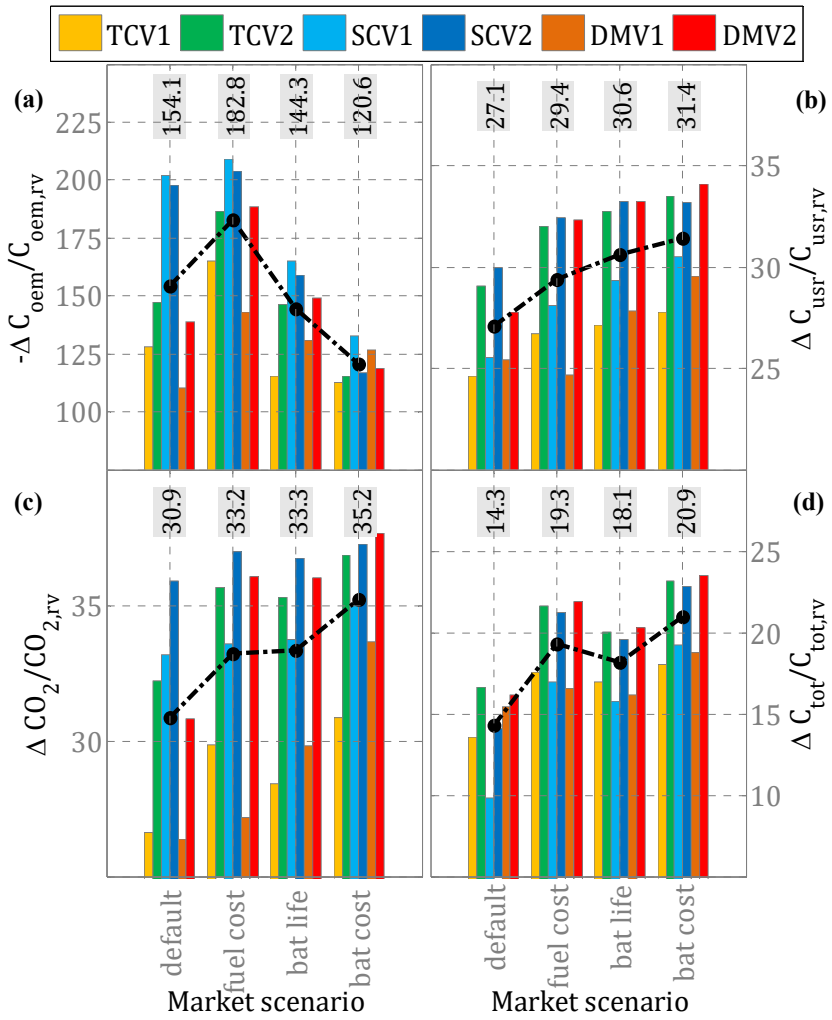

Figure 11 – Increase in OEM costs (a), decrease in user costs (b), in CO2 emissions (c) and in total costs (d) for different market scenarios and for each type of vehicle.

In an increasing fuel cost scenario (second group of bars in the charts in Fig. 11), the optimization is in particular aimed at reducing CO2 emissions, even though more batteries would be required during the life of the vehicle. However, this strategy has an important effect on the OEM costs, which rise to 182.8% (Fig. 11a) compared to the reference vehicle. The results obtained for the market scenario in which the battery cost is halved (fourth group of bars in Fig. 11) indicate that the battery cost is the most significant factor in promoting the hybrid technology. In fact, in this scenario, the average OEM cost increase is the lowest one (120.6%), the average CO2

900 emission reduction is the highest one (35.2%) and the average total cost reduction, with respect to the
901 conventional vehicle, is the highest one (20.9%). The scenario in which the battery duration is increased (third
902 group of bars in Fig. 11) also leads to a significant improvement in the performance of the hybrid vehicles.
903 It is worth observing that each architecture that is equipped with the D2 engine leads to the lowest total costs for
904 the three speculated market conditions.
905 In order to conclude the analysis, Figure 12 reports the distribution of the best vehicles that were selected for
906 different driving-configurations using two target functions (ratio between the CO2 reduction and OEM cost
907 increase $\frac{\Delta CO_2}{\Delta C_{oem}}$ in the left column, total powertrain cost, C_{tot} in the right column) and exploring the four market
908 scenarios, namely the default scenario (Fig. 12a), the scenario in which the fuel cost is increased by 50% (Fig.
909 12b), the scenario in which the battery life is increased by 50% (Fig. 12c) and, finally, the scenario in which the
910 battery-cost is halved (Fig. 12d).
911 It can be observed that, as far as the $\frac{\Delta CO_2}{\Delta C_{oem}}$ target function is considered, DMVs are the best architectures in the
912 incremented fuel-cost scenario, while DMV-D1 is better in the low-medium energy region. TCVs and DMV-D2
913 are instead better if a battery with a longer life is expected to be available on the market (Fig. 12c).
914 The scenario in which the battery cost is halved suggests choosing the D2 engine and the speed coupling
915 architecture (Fig. 12d). In particular, SCV-D2 is convenient in the medium-high velocity and low-medium
916 energy region, while TCV-D2 is convenient in the TM1-TM3-AUDC region.
917 However, if the total cost reduction is the only target (right column in Fig. 12), each market scenario promotes
918 the selection of DMV-D2 in most of the regions, while SCV-D2 is selected in the low energy demand region.
919 The size of the components of each vehicle is reported in Table 6 for the set of vehicles and for the four market
920 scenarios.

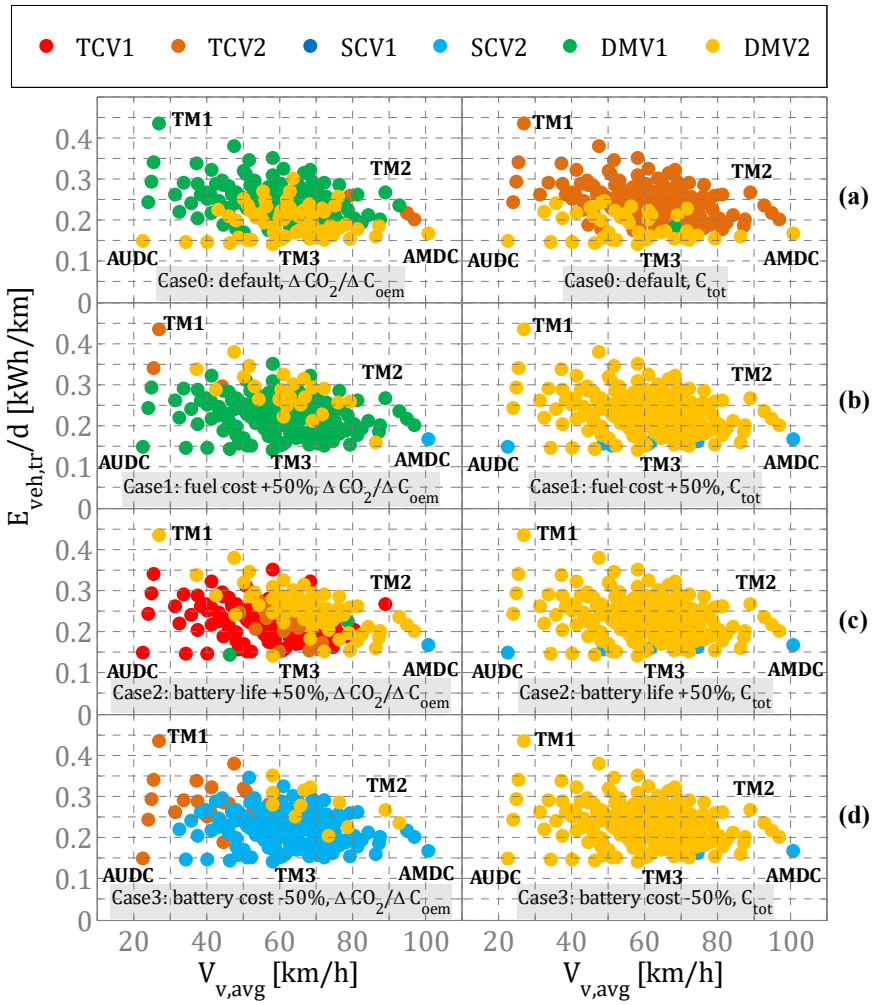

Figure 12 – Optimal hybrid architectures selected over several driving conditions, for different market scenarios and target functions.

The main outcome concerns the speed ratio of the TC device, which is increased to 1.7 in each new condition for DMV-D2, in order to better exploit the battery component for both regenerative braking and pure electric traction. Higher TC speed ratios in fact lead to a more intense battery employment, which directly affects the battery replacement costs and therefore both the OEM and the total costs. However, in the fuel cost increase scenario (case 1), the battery cost contribution is less important, and both the design and the control strategy are aimed at the reduction of CO2 emissions.

Moreover, if the battery life increases or the battery cost decreases (cases 2 and 3, respectively), the economic impact of the battery component is always lower, whatever strategy is defined.

Table 6 – Design of the set of vehicles for the four market scenarios, in terms of the maximum power of the engine, battery and EM (kW) and of the TC, SC and FD ratios.

			Engine power (kW)	Battery power (kW)	EM power (kW)	TC speed ratio	SC speed ratio	FD speed ratio
D1	**TCV**	**Default**	100	30	30	0.59		3.25
		Fuel cost	100	32.5	32.5	0.8		3.25
		Battery life	100	30	30	0.8		3.25
		Battery cost	100	35	35	0.5		3.25
	SCV	**Default**	100	32.5	32.5		2.7	2.5
		Fuel cost	100	32.5	32.5		2.7	2.5
		Battery life	100	35	35		2.7	2.5
		Battery cost	100	35	35		2.7	2.5
	DMV	**Default**	100	27.5	27.5	0.5	4.5	2.5
		Fuel cost	100	27.5	27.5	0.5	4.2	2.75
		Battery life	100	30	30	0.5	3	2.5
		Battery cost	100	35	35	0.8	3.9	2.75
D2	**TCV**	**Default**	70	42.5	42.5	0.91		3.25
		Fuel cost	70	47.5	47.5	1.7		3.25
		Battery life	70	45	45	1.7		3.25
		Battery cost	70	45	45	1.7		3.25
	SCV	**Default**	70	50	50		3	2.5
		Fuel cost	70	47.5	47.5		3	2.5
		Battery life	70	45	45		3	2.5
		Battery cost	70	40	40		2.7	2.5
	DMV	**Default**	70	40	40	0.5	4.2	2.5
		Fuel cost	70	47.5	47.5	1.7	4.2	2.5
		Battery life	70	45	45	1.7	4.2	2.5
		Battery cost	70	45	45	1.7	3.9	2.5

8. Conclusion and future work

This present study has focused on the refinement of a previously developed tool for the definition of the optimal layout in hybrid vehicles, based on powertrain cost reduction, and on its application to a newly proposed non-plug-in parallel hybrid architecture that is able to incorporate torque-coupling (TC) and speed-coupling (SC) functions, and is therefore referred to as a dual-mode vehicle (DMV). The performance of this architecture has been evaluated in detail in terms of cost and CO2 emission reduction with respect to a conventional vehicle. Two different diesel engines, which are here referred to as D1 and D2 (with displacements of 1.7L and 1.3L, respectively), have been considered for the design optimization process. A bi-level (nested) tool has been developed for the simultaneous optimization of the vehicle design and control strategy to manage the power flow of the engine and electric machines. The tool identifies the optimal layout by minimizing the powertrain cost over the lifetime of the vehicle. Different cost definitions have been considered in this study: production costs (C_{pr}), which account for the production cost required by the OEM; OEM costs (C_{oem}), which consist of the production cost and a fraction of the cost due to battery replacement over the vehicle lifetime; fuel costs (C_{fc}), which are related to the fuel consumed; operating costs (C_{op}), which consist of the fuel cost and the battery replacement cost; user costs (C_{usr}), which include the fuel cost and a fraction of the battery replacement costs (this is basically an operating cost-oriented definition, as it does not include the cost required to purchase the vehicle and the costs related to insurance/taxes); total costs (C_{tot}), which are the sum of the production cost and the operating cost.

A sensitivity analysis has been carried out in order to verify the impact of the cost definition, of the objective function and of the training mission typology on the resulting optimal layout and its performance, in terms of CO2 and pollutant emission reduction, as well as in terms of cost reduction. In addition, different market scenarios, which consider a fuel price increment (+50%), a longer battery life (+50%) and a battery cost decrement (-50%), have been explored individually in terms of optimal layout and the resulting performance. The main findings of this study can be summarized as follows:

1. Vehicle architectures: The dual-mode vehicle equipped with the smallest engine D2 (i.e., DMV-D2) shows the best potential to reduce the total costs (an average 15.9% reduction) with limited penalties in terms of incremental OEM costs with respect to the conventional vehicle (139%), and a good performance in terms of CO2 reduction (30%). The speed-coupling vehicle equipped with the D2 engine (i.e, SCV-D2) shows a higher CO2 reduction potential (35.5%), but at the expense of a higher increment in the OEM costs (197.9%).
2. Sensitivity analysis on the powertrain cost definition: The total powertrain cost definition C_{tot} was selected as the best choice when defining the optimal layout of the hybrid vehicle, as it leads to the lowest incremental OEM costs per unit CO2 emission reduction, per unit user cost reduction and per unit total powertrain cost reduction. However, fuel cost or user cost definitions could also be used to define the optimal layout if a more intense CO2 emission reduction is necessary, regardless of the increment in the powertrain costs. If the C_{tot} definition is selected for layout optimization, the average powertrain cost reduction is about 12.4%, CO2 emissions are reduced by 31.4%, and the OEM cost increase is 123%. If the C_{oem} definition is used, the resulting HEV layouts provide similar results to those obtained with total cost approach. If C_{usr} or C_{fc} are minimized, the resulting HEV layout shows the best potential to reduce the CO_2 emissions (by as much as 35%), but at the expense of a higher battery usage and the related costs (the C_{tot} reduction is limited to 10-11%). An interesting indicator that was investigated is the ratio between the incremental C_{oem} and the achieved CO2 emission reduction unit. It was found that the increased OEM cost, due to a reduction of 1g/km of CO2 emissions, was estimated to be around $44 per vehicle, if the layout was selected using the OEM cost definition, while it was around $55 per vehicle, if the layout was selected using the user cost definition.
3. Sensitivity analysis of the objective function: the objective function oriented toward fuel consumption and battery depletion resulted to be the most balanced choice to define the vehicle control strategy during the layout optimization process. If an NO_x-oriented objective function is used, the layout results to be optimized for the extensive use of the electric power unit, in order to shift the engine operating point to a low NO_x emission region. However, this leads to high battery depletion.

4. Analysis of the different market scenarios: in a scenario in which the fuel cost increases by 50% with respect to the nominal value adopted in this study, the layout optimization is in particular aimed at reducing CO2 emissions, even though more batteries would be required during the lifetime of the vehicle. However, this strategy has a drastic effect on the OEM cost increase, which rises to 182.8% (against a nominal value of 154.1%). The battery cost resulted to be the most significant factor in promoting the hybrid technology. In the scenario in which the battery cost is halved, the average OEM cost increment is in fact the lowest (120.6%), the average CO2 emission reduction is the highest (35.2%) and the average total cost reduction is the highest one (20.9%). The proposed DMV architecture was found to be the best choice to reduce the overall powertrain costs, for all the considered scenarios related to fuel price increase, battery life increase and battery cost decrease.

Finally, some topics and ideas for future investigations have emerged from this study and they will be investigated in detail in the near future. For example, the optimal vehicle design toolbox is intended to also be applied to complex plug-in and non-plug-in hybrid electric vehicles. Moreover, a new algorithm for an equivalent consumption minimization strategy (ECMS) that takes into account the battery life consumption is currently under investigation for DMVs. A comprehensive optimization tool, which is capable of identifying not only the optimal control strategy of the hybrid powertrains over the mission, but also the optimal values of the main engine parameters (i.e., EGR rate, start of injection), is currently being developed. This tool will incorporate specifically developed low-throughput models that simulate the combustion and emission formation processes in the engine.

Acknowledgements

General Motors PowerTrain Europe is gratefully acknowledged for the technical support.

References

[1] K. D. Huang, K. V. Quang, K.-T. Tseng, Study of the effect of contraction of cross-sectional area on flow energy merger in hybrid pneumatic power system, Applied Energy 86 (10):2171–2182, 2009, doi:10.1016/j.apenergy.2009.03.002.

[2] M. Hannan, F. Azidin, A. Mohamed, Hybrid electric vehicles and their challenges: A review, Renewable and Sustainable Energy Reviews 29:35–150, 2014, doi: 10.1016/j.rser.2013.08.097.

[3] W. Liu, W. Hu, H. Lund, Z. Chen, Electric vehicles and large-scale integration of wind power–the case of inner mongolia in china, Applied Energy 104:445–456, 2013, doi: 10.1016/j.apenergy.2012.11.003.

[4] X. Wu, B. Cao, X. Li, J. Xu, X. Ren, Component sizing optimization of plug-in hybrid electric vehicles, Applied Energy 88 (3):799–804, 2011, doi:10.1016/j.apenergy.2010.08.018.

[5] K. Ç. Bayindir, M. A. Gözüküçük, A. Teke, A comprehensive overview of hybrid electric vehicle: Powertrain configurations, powertrain control techniques and electronic control units, Energy Conversion and Management 52 (2):1305–1313, 2011, doi: 10.1016/j.enconman.2010.09.028.

[6] L. Damiani, M. Repetto, A. P. Prato, Improvement of powertrain efficiency through energy breakdown analysis, Applied Energy 121:252–263, 2014, doi: 10.1016/j.apenergy.2013.12.067.

[7] S. Saxena, A. Phadke, A. Gopal, Understanding the fuel savings potential from deploying hybrid cars in china, Applied Energy 113:1127–1133, 2014, doi: 10.1016/j.apenergy.2013.08.057.

[8] S. Zhang, Y. Wu, H. Liu, R. Huang, L. Yang, Z. Li, L. Fu, J. Hao, Real-world fuel consumption and CO2 emissions of urban public buses in Beijing, Applied Energy 113:1645–1655, 2014, doi: 10.1016/j.apenergy.2013.09.017.

[9] T. Hutchinson, S. Burgess, G. Herrmann, Current hybrid-electric powertrain architectures: Applying empirical design data to life cycle assessment and whole-life cost analysis, Applied Energy 119: 314–329, 2014, doi: 10.1016/j.apenergy.2014.01.009.

[10] T. Katrašnik, Impact of vehicle propulsion electrification on well-to-wheel CO2 emissions of a medium duty truck, Applied Energy 108:236–247, 2013, doi: 10.1016/j.apenergy.2013.03.029.

[11] B. M. Al-Alawi, T. H. Bradley, Analysis of corporate average fuel economy regulation compliance scenarios inclusive of plug in hybrid vehicles, Applied Energy 113:1323–1337, 2014, doi: 10.1016/j.apenergy.2013.08.081.

[12] R. T. Doucette, M. D. McCulloch, Modeling the prospects of plug-in hybrid electric vehicles to reduce CO2 emissions, Applied Energy 88 (7):2315–2323, 2011, doi: 10.1016/j.apenergy.2011.01.045.

[13] X. Wu, J. Dong, Z. Lin, Cost analysis of plug-in hybrid electric vehicles using GPS-based longitudinal travel data, Energy Policy 68 :206–217, 2014, doi: 10.1016/j.enpol.2013.12.054.

[14] H. K. Fathy, J. Reyer, P. Y. Papalambros, A. Ulsov, et al., On the coupling between the plant and controller optimization problems, in: American Control Conference, 2001. Proceedings of the 2001, Vol. 3, IEEE, 2001, pp. 1864–1869, doi: 10.1109/ACC.2001.946008.

[15] M. Jain, C. Desai, S. S. Williamson, Genetic algorithm based optimal powertrain component sizing and control strategy design for a fuel cell hybrid electric bus, in: Vehicle Power and Propulsion Conference, 2009. VPPC'09. IEEE, IEEE, 2009, pp. 980–985, doi: 10.1109/VPPC.2009.5289740.

[16] M.-J. Kim, H. Peng, Power management and design optimization of fuel cell/battery hybrid vehicles, Journal of power sources 165 (2): 819–832, 2007, doi: 10.1109/TCST.2003.815606.

[17] Z. Yu, D. Zinger, A. Bose, An innovative optimal power allocation strategy for fuel cell, battery and supercapacitor hybrid electric vehicle, Journal of Power Sources 196 (4) : 2351–2359, 2011, doi: doi:10.1016/j.jpowsour.2010.09.057.

[18] V. Paladini, T. Donateo, A. De Risi, D. Laforgia, Super-capacitors fuel-cell hybrid electric vehicle optimization and control strategy development, Energy Conversion and Management 48 (11) : 3001–3008, 2007, doi: doi:10.1016/j.enconman.2007.07.014.

[19] K.-B. Sheu, Simulation for the analysis of a hybrid electric scooter powertrain, Applied energy 85 (7):589–606, 2008, doi: doi:10.1016/j.apenergy.2007.09.002.

[20] S.-C. Tzeng, K. D. Huang, C.-C. Chen, Optimization of the dual energy-integration mechanism in a parallel-type hybrid vehicle, Applied Energy 80 (3): 225–245, 2005, doi: doi:10.1016/j.apenergy.2004.04.010.

[21] G. Paganelli, Y. Guezennec, G. Rizzoni, Optimizing control strategy for hybrid fuel cell vehicle, Tech. rep., SAE Technical Paper 2002-01-0102, 2002, doi:10.4271/2002-01-0102.

[22] R. Bellman, R. E. Kalaba, Dynamic programming and modern control theory, Academic Press New York, 1965.

[23] W. L. Winston, J. B. Goldberg, Operations research: applications and algorithms, Vol. 3, Duxbury press Boston, 2004.

[24] O. Sundström, L. Guzzella, A generic dynamic programming matlab function, in: Control Applications,(CCA) & Intelligent Control,(ISIC), 2009 IEEE, IEEE, 2009, pp. 1625–1630, doi: 10.1109/CCA.2009.5281131.

[25] Finesso, R., Spessa, E., & Venditti, M., Optimization of the Layout and Control Strategy for Parallel Through-the-Road Hybrid Electric Vehicles, SAE Technical Paper 2014-01-1798, 2014, doi:10.4271/2014-01-1798.

[26] Finesso, R., Spessa, E., & Venditti, M., Layout design and energetic analysis of a complex diesel parallel hybrid electric vehicle, Applied Energy, 134: 573-588, 2014, doi:10.1016/j.apenergy.2014.08.007.

[27] MathWorks, MatLab - The Language Of Technical Computing, http://www.mathworks.com/products/matlab/, [Online; accessed 04-May-2016] (2016).

[28] Finesso, R., Spessa, E., & Venditti, M., An Unsupervised Machine-Learning Technique for the Definition of a Rule-Based Control Strategy in a Complex HEV, SAE Int. J. Alt. Power. 5(2):2016, doi:10.4271/2016-01-1243.

[29] S. d'Ambrosio, R. Finesso, E. Spessa, Calculation of mass emissions, oxygen mass fraction and thermal capacity of the inducted charge in SI and diesel engines from exhaust and intake gas analysis, Fuel 90 (1):152–166, 2011, doi:10.1016/j.fuel.2010.08.025.

[30] J. B. Heywood, Internal combustion engine fundamentals, Vol. 930, Mcgrawhill New York, 1988.

[31] U. Technologies, http://www.uqm.com, [Online; accessed 04-May-2016] (2016).

[32] Serrao, L., Onori, S., Sciarretta, A., Guezennec, Y., & Rizzoni, G. (2011, June). Optimal energy management of hybrid electric vehicles including battery aging. In American Control Conference (ACC), 2011 (pp. 2125-2130). IEEE, 10.1109/ACC.2011.5991576.

[33] Golbuff, S., Design Optimization of a Plug-In Hybrid Electric Vehicle, SAE Technical Paper 2007-01-1545, 2007, doi:10.4271/2007-01-1545.

[34] Fischer, R., Fraidl, G., Hubmann, C., Kapus, P., Kunvemann, R., Sifferlinger, B., & Beste, F, Range Extender Module - Enabler for Electric Mobility, ATZ autotechnology, 9, 2009.

[35] Catania, A. E., Finesso, R., & Spessa, E., Predictive zero-dimensional combustion model for DI diesel engine feed-forward control. Energy Conversion and Management, 52(10): 3159-3175, 2011, doi:10.1016/j.enconman.2011.05.003.

[36] Morra, E. P., Spessa, E., & Venditti, M. (2012, May). Optimization of the operating strategy of a BAS hybrid diesel powertrain on type-approval and real-world representative driving cycles. In ASME 2012 internal combustion engine division spring technical conference (pp. 557-568). American Society of Mechanical Engineers, doi: doi:10.1115/ICES2012-81093.

[37] Morra, E., Spessa, E., Ciaravino, C., & Vassallo, A., Analysis of various operating strategies for a parallel-hybrid diesel powertrain with a belt alternator starter, SAE Int. J. Alt. Power. 1(1):231-239, 2012, doi:10.4271/2012-01-1008.

[38] Catania, A., Finesso, R., Spessa, E., Catanese, A., & Landsmann, G., Combustion prediction by a low-throughput model in modern diesel engines, SAE Int. J. Engines 4(1):2106-2123, 2011, doi:10.4271/2011-01-1410.

[39] Catania, A., Finesso, R., & Spessa, E., Real-time calculation of EGR rate and intake charge oxygen concentration for misfire detection in diesel engines, SAE Technical Paper 2011-24-0149, 2011, doi:10.4271/2011-24-0149.

[40] Finesso, R., & Spessa, E., Real-Time Predictive Modeling of Combustion and NO x Formation in Diesel Engines Under Transient Conditions (No. 2012-01-0899). SAE Technical Paper 2012-01-0899, 2012, doi:10.4271/2012-01-0899.